SUPPORTING INFORMATION

The Influence of Hydrophobicity on Excitonic Coupling in DNA-Templated Indolenine Squaraine Dye Aggregates

Olga A. Mass,[1] Christopher K. Wilson,[1] German Barcenas,[1] Ewald. A Terpetschnig,[2] Olena M. Obukhova,[3] Olga S. Kolosova,[3] Anatoliy L. Tatarets,[3] Lan Li,[1,4] Bernard Yurke,[1,5] William B. Knowlton,[1,5] Ryan. D. Pensack,[1,*] and Jeunghoon Lee.[1,6,*]

[1]Micron School of Materials Science & Engineering, [5]Department of Electrical & Computer Engineering, [6]Department of Chemistry and Biochemistry, Boise State University, Boise, Idaho 83725, United States

[2]SETA BioMedicals, LLC, 2014 Silver Court East, Urbana, IL 61801, United States

[3]State Scientific Institution "Institute for Single Crystals" of National Academy of Sciences of Ukraine, Kharkiv, 61072, Ukraine

[4]Center for Advanced Energy Studies, Idaho Falls, ID 83401, USA

Corresponding authors:

*jeunghoonlee@boisestate.edu
*ryanpensack@boisestate.edu

Table of Contents

Supporting Information 1: *Squaraine Chemical Synthesis*

General

The phosphate buffer pH 7.4 (67 mM) (PB) was prepared by dissolving $Na_2HPO_4 \cdot 2H_2O$ (9.596 g) and KH_2PO_4 (1.743 g) in 1 L of Milli-Q water. Bicarbonate buffer of pH 9.0 (0.1 mM) was obtained by dissolving $NaHCO_3$ (8.401 g) in 1 L of Milli-Q water.

The **C, H, N elemental analysis** was performed by a EuroVector Euro EA 3000 EA-IRMS elemental analyzer.

^{1}H NMR spectra were measured on a *Varian Mercury-VX-200* (^{1}H 200 MHz) or Varian 400 MR (^{1}H 400 MHz) spectrometer in DMSO-d_6 using signal of remaining non-deuterated solvent as an internal standard (2.50 ppm for DMSO).

ESI mass spectra were recorded on *Waters Quattro micro API* mass spectrometer with direct injection of the sample solution to the ionization chamber.

Absorption spectra were recorded in 1-cm quartz cells at 25 ºC using a PerkinElmer Lambda 35 UV/Vis spectrophotometer. Absorption maxima were determined with an accuracy of ±0.5 nm and rounded off.

2-((1-(5-carboxypentyl)-3,3-dimethylindolin-2-ylidene)methyl)-3-oxo-4-((1,3,3-trimethyl-3*H*-indol-1-ium-2-yl)methylene)cyclobut-1-en-1-olate (**SQ-H$_2$-COOH**).

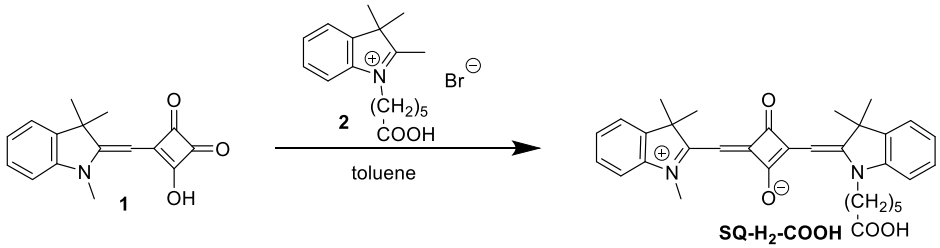

3-Hydroxy-4-((1,3,3-trimethylindolin-2-ylidene)methyl)cyclobut-3-ene-1,2-dione (**1**) (150 mg, 0.56 mmol) and 1-(5-carboxypentyl)-2,3,3-trimethyl-3H-indolium bromide (**2**) (200 mg, 0.56 mmol) were heated under reflux in toluene (10 mL) for 10 h. The solvent was removed under reduced pressure by rotary evaporation. The residue was purified using column chromatography (Silica gel 60, 0–8% methanol—chloroform) to give **SQ-H$_2$-COOH** (190 mg, 65%) as a dark blue solid with a golden sheen. ^{1}H-NMR (200 MHz, DMSO-d$_6$), δ, ppm: 7.52 (2H, d, 7.3 Hz, arom.), 7.44–7.25 (4H, m, arom.), 7.25–7.04 (2H, m, arom.), 5.79 (1H, s, CH), 5.76 (1H, s, CH), 4.06 (2H, t, 7.4 Hz, NCH_2), 3.57 (3H, s, NCH_3), 2.21 (2H, t, 6.7 Hz, $C\underline{H_2}COOH$), 1.68 (12H, s, $(CH_3)_2$), 1.80–1.29 (6H, m). MALDI-TOF MS, m/z calcd. for $[C_{33}H_{36}N_2O_4]$ 524.27, found: 525.32 $[M+H]^+$. Anal. calcd. (%) for $C_{33}H_{36}N_2O_4$: C, 75.55; H, 6.92; N, 5.34. Found C, 75.43; H, 6.89; N, 5.31. UV-Vis: λ_{max}(Abs) 630 nm (Methanol); λ_{max}(Em) 639 nm (Methanol); λ_{max}(Abs) 622 nm, ε 285,000 $M^{-1}cm^{-1}$ (Phosphate buffer); λ_{max}(Em) 632 nm (Phosphate buffer).

2-((1-(5-carboxypentyl)-5-chloro-3,3-dimethylindolin-2-ylidene)methyl)-4-((5-chloro-1,3,3-trimethyl-3*H*-indol-1-ium-2-yl)methylene)-3-oxocyclobut-1-en-1-olate (SQ-Cl$_2$-COOH).

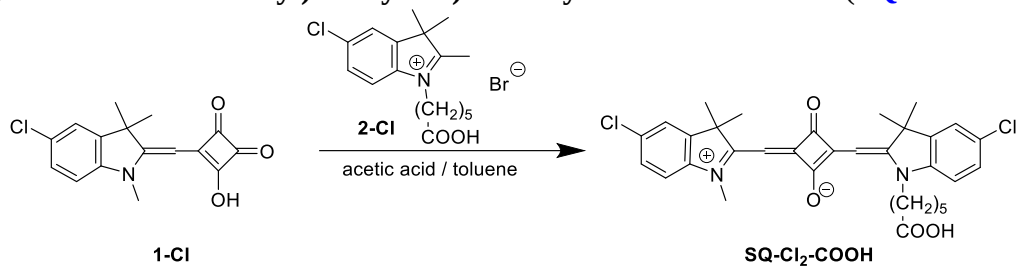

3-((5-Chloro-1,3,3-trimethylindolin-2-ylidene)methyl)-4-hydroxycyclobut-3-ene-1,2-dione (**1-Cl**) (240 mg, 0.79 mmol) and 1-(5-carboxypentyl)-5-chloro-2,3,3-trimethyl-3*H*-indol-1-ium bromide (**2-Cl**) (306 mg, 0.79 mmol) were heated under reflux in a mixture of acetic acid (5 mL) and toluene (15 mL) for 24 h. The solvent was removed under reduced pressure by rotary evaporation. The residue was purified using column chromatography (Silica gel 60, 0–4% methanol—chloroform) to give **SQ-Cl$_2$-COOH** (97 mg, 21%) as a dark blue solid. ^{1}H-NMR (400 MHz, DMSO-d$_6$), δ, ppm: 7.66 (2H, s, arom.), 7.44–7.30 (4H, m, arom.), 5.79 (1H, s, CH), 5.76 (1H, s, CH), 4.11–4.00 (2H, broad s, NCH$_2$), 3.56 (3H, s, NCH$_3$), 2.20 (2H, t, 6.8 Hz, CH$_2$COOH), 1.68 (12H, s, (CH$_3$)$_2$), 1.60–1.48 (2H, m, CH$_2$), 1.41–1.33 (2H, m, CH$_2$), 1.26–1.18 (2H, m, CH$_2$). ESI MS, m/z calcd. for [C$_{33}$H$_{34}$Cl$_2$N$_2$O$_4$] 592.19, found: 593.28 (100%), 595.27 (64%) [M+H]$^+$. Anal. calcd. (%) for C$_{33}$H$_{34}$Cl$_2$N$_2$O$_4$: C, 66.67; H, 5.93; N, 4.71. Found C, 66.78; H, 5.99; N, 4.67. UV-Vis: λ_{max}(Abs) 633 nm, ε 250,000 M^{-1}cm^{-1} (Methanol); λ_{max}(Em) 644 nm (Methanol).

2-((1-(5-carboxypentyl)-3,3-dimethyl-5-sulfoindolin-2-ylidene)methyl)-3-oxo-4-((1,3,3-trimethyl-5-sulfo-3*H*-indol-1-ium-2-yl)methylene)cyclobut-1-en-1-olate (SQ-Sl$_2$-COOH).

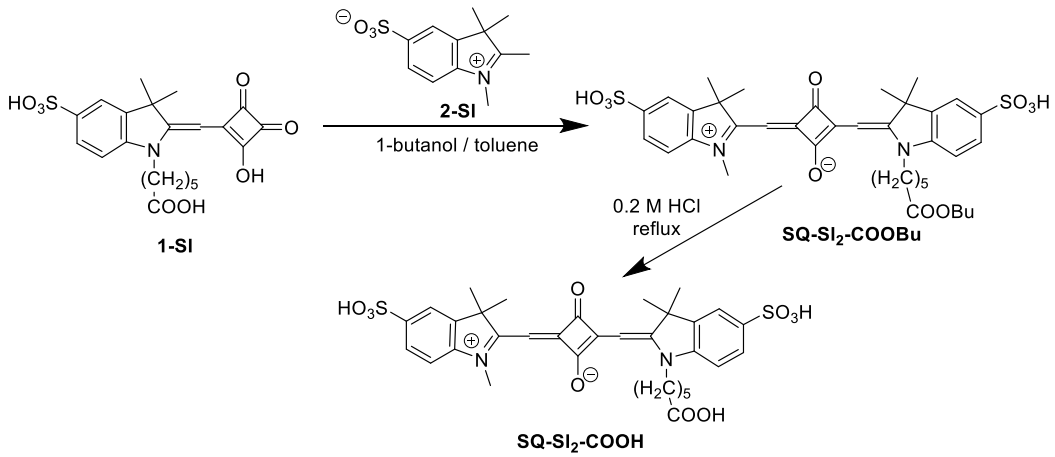

6-(2-((2-hydroxy-3,4-dioxocyclobut-1-en-1-yl)methylene)-3,3-dimethyl-5-sulfoindolin-1-yl)hexanoic acid (**1-Sl**) (225 mg, 0.50 mmol) and 1,2,3,3-tetramethyl-3H-indol-1-ium-5-sulfonate (**2-Sl**) (127 mg, 0.50mmol) were heated under reflux in a mixture of 1-butanol (5 mL) and toluene (3 mL) for 8 h. The solvent was removed under reduced pressure by rotary evaporation. The residue containing butyl ester of the dye (**SQ-Sl$_2$-COOBu**) was hydrolyzed in 0.2 M hydrochloric acid (50 mL) at 100 °C for 30 min. The water was evaporated under reduced pressure and the product was purified using column chromatography (Silica gel 60 RP18, 0–14% acetonitrile—water) to give **SQ-Sl$_2$-COOH** (215 mg, 62%) as a dark blue solid. ^{1}H-NMR (400 MHz, DMSO-

d_6), δ, ppm: 7.66 (2H, s, arom.), 7.62–7.57 (2H, m, arom.), 7.30 – 7.23 (2H, m, arom.), 5.81 (1H, s, CH), 5.77 (1H, s, CH), 4.08 (2H, broad s, NCH_2), 3.58 (3H, s, NCH_3), 2.21 (2H, t, 6.7 Hz, CH_2COOH), 1.74–1.64 (2H, m, CH_2), 1.68 (12H, s, $(CH_3)_2$), 1.60–1.45 (2H, m, CH_2), 1.43–1.34 (2H, m, CH_2). ESI MS, m/z calcd. for $[C_{33}H_{36}N_2O_{10}S_2]$ 684.18, found: 685.32 $[M+H]^+$. Anal. calcd. (%) for $C_{33}H_{36}N_2O_{10}S_2$: C, 57.88; H, 5.30; N, 4.09. Found C, 57.93; H, 5.28; N, 4.14. UV-Vis: λ_{max}(Abs) 628 nm, ε 290,000 $M^{-1}cm^{-1}$ (Phosphate buffer); λ_{max}(Em) 640 nm (Phosphate buffer).

2-((1-(5-carboxypentyl)-3,3,5-trimethylindolin-2-ylidene)methyl)-3-oxo-4-((1,3,3,5-tetramethyl-3*H*-indol-1-ium-2-yl)methylene)cyclobut-1-en-1-olate (**SQ-Me$_2$-COOH**).

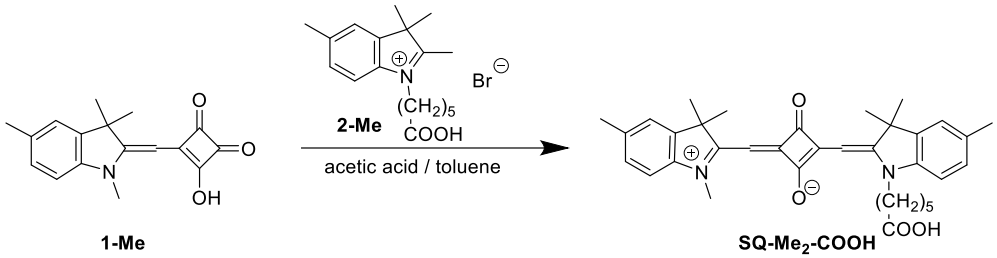

3-Hydroxy-4-((1,3,3,5-tetramethylindolin-2-ylidene)methyl)cyclobut-3-ene-1,2-dione (**1-Me**) (186 mg, 0.66 mmol) and 1-(5-carboxypentyl)-2,3,3,5-tetramethyl-3*H*-indol-1-ium bromide (**2-Me**) (242 mg, 0.66 mmol) were heated under reflux in a mixture of acetic acid (5 mL) and toluene (20 mL) for 18 h. The solvent was removed under reduced pressure by rotary evaporation. The residue was purified using column chromatography (Silica gel 60, 0–1% methanol—chloroform) to give **SQ-Me$_2$-COOH** (137 mg, 38%) as a dark blue solid with a golden sheen. ^{1}H-NMR (400 MHz, DMSO-d_6), δ, ppm: 7.32 (2H, s, arom.), 7.23–7.12 (4H, m, arom.), 5.74 (1H, s, CH), 5.70 (1H, s, CH), 4.04 (2H, broad s, NCH_2), 3.54 (3H, s, NCH_3), 2.35 (6H, s, CH_3), 2.20 (2H, t, 6.7 Hz, CH_2COOH), 1.75–1.62 (2H, m, CH_2), 1.66 (12H, s, $(CH_3)_2$), 1.59–1.51 (2H, m, CH_2), 1.42–1.35 (2H, m, CH_2). ESI MS, m/z calcd. for $[C_{35}H_{40}N_2O_4]$ 552.30, found: 553.42 $[M+H]^+$. Anal. calcd. (%) for $C_{35}H_{40}N_2O_4$: C, 76.06; H, 7.29; N, 5.07. Found C, 76.18; H, 7.33; N, 5.14. UV-Vis: λ_{max}(Abs) 635 nm; λ_{max}(Em) 646 nm (Methanol).

General procedure for the synthesis of the N-Hydroxysuccinimide ester of **SQ-R$_2$-COOH** (**SQ-R$_2$-NHS**).

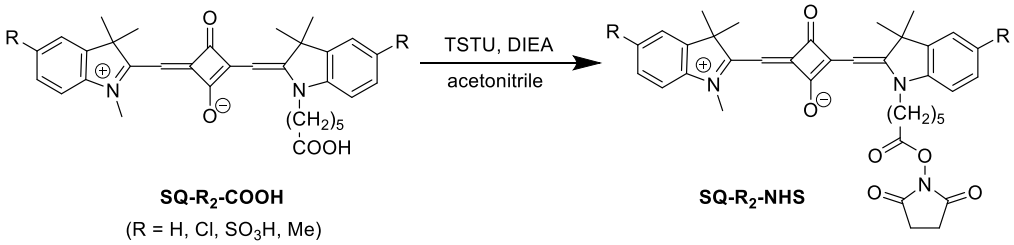

SQ-R$_2$-COOH (57 μmol), *N*,*N*,*N*′,*N*′-tetramethyl-*O*-(*N*-succinimidyl)uronium tetrafluoroborate (TSTU) (26 mg, 86 μmol), and *N*,*N*-diisopropylethylamine (DIEA) (16 μL, 92 μmol) were dissolved in acetonitrile (3 mL). The solution was stirred at room temperature for 20 min. The solvent was removed under reduced pressure by rotary evaporation. The residue was purified using column chromatography (Silica gel 60, 0–3% methanol—chloroform) to give **SQ-R$_2$-NHS**.

General procedure for oligonucleotide post-modification with a squaraine dye (performed at Integrated DNA Technologies, Inc., Coralville, IA)

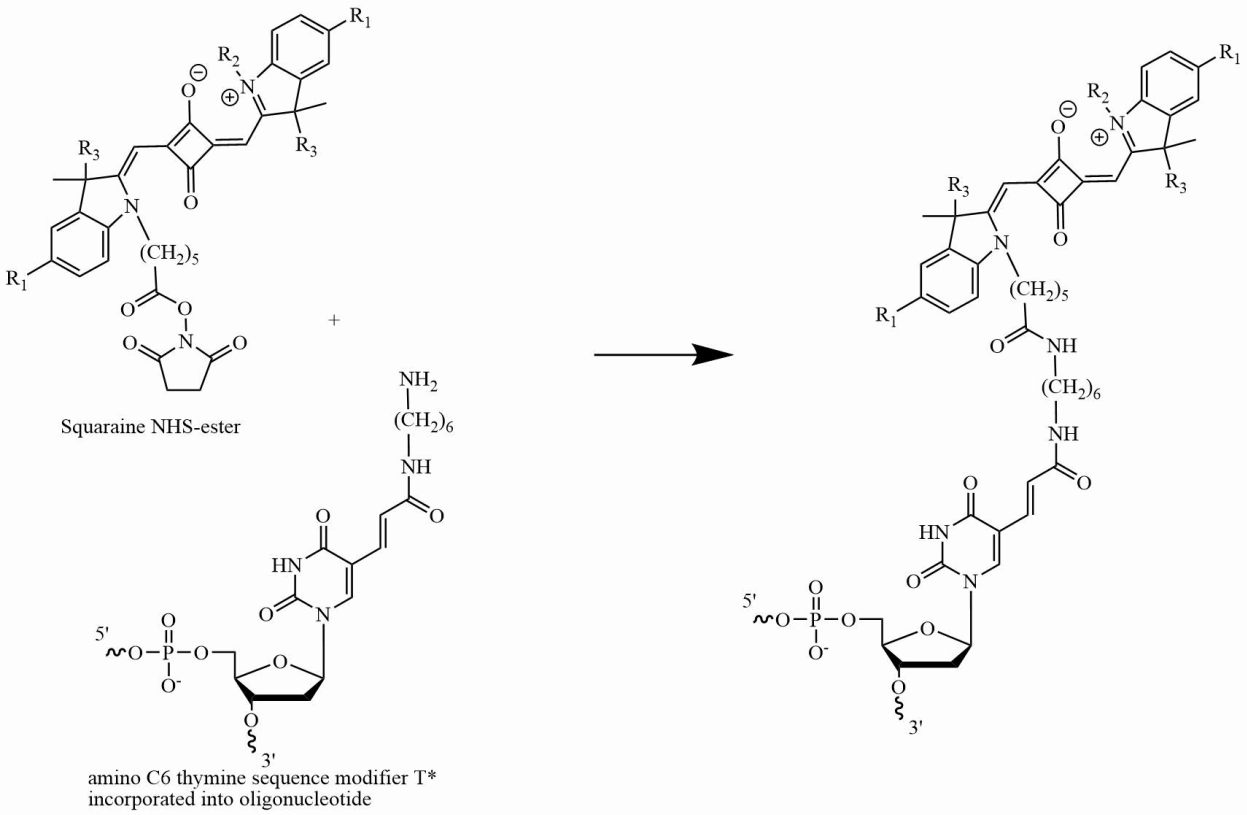

Supporting Information 2: *Electrophoretic Analysis*

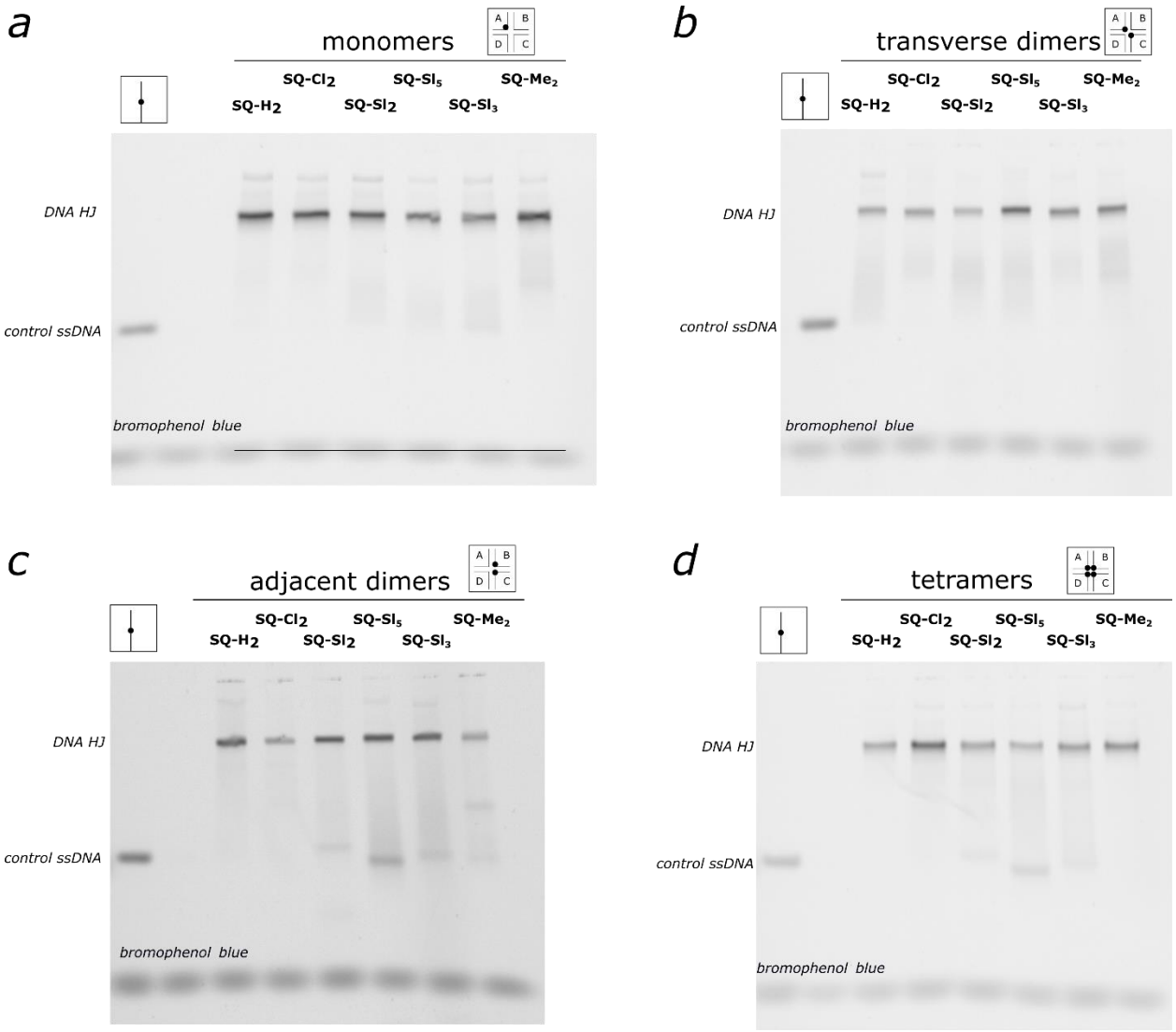

Figure S1. Fluorescent images of 15% nondenaturing PAGE, 1.5 mm of (**a**) squaraine monomers; (**b**) squaraine transverse dimer run; (**c**) squaraine adjacent dimer; and (d) squaraine tetramers. The gels were run at 150 V, 17 ºC in 1× TBE, 15 mM $MgCl_2$. Squaraine-DNA HJ (0.15 μM, 10 μL) were run against ssDNA covalently labeled with **SQ-H2** as a control (0.075 μM, 10 μL). Note that as fluorescence of squaraine aggregates is highly suppressed.

Nondenaturing PAGE was carried out to evaluate the formation of DNA HJ templaitng squaraine aggregates. The 15% non-denaturing electrophoresis gel, 1.5 mm was casted in 1× TBE, 15 mM $MgCl_2$. DNA samples were diluted 10-fold in Loading Buffer [Ficoll (SigmaAldrich) 20% v/v, bromophenol blue (SigmaAldrich) 20% v/v]. The DNA HJ samples were loaded on the gel at DNA concentration 0.15 μM alongside with three ssDNA controls at 0.075 μM. PAGE was run for ~ 1 h 40 min at 150 V constant voltage at 17 °C constant temperature in running buffer 1× TBE, 15 mM $MgCl_2$. The electrophoresed gel was scanned in FluorChem Q imager (Alpha Innotech) in the Cy5-channel (ex. 632 nm; em. 691 nm).

Supporting Information 3: *Thermal Denaturation*

Thermal denaturation (melting) profiles of squaraine-DNA constructs were recorded using a Varian Cary5000 spectrophotometer equipped with a thermal probe (Agilent Technologies Cary Temperature Controller G9808). Prior to measurements, samples were degassed for 5 min at room temperature in a vacuum centrifuge. Samples were equilibrated at 25 °C for 2 min before starting a temperature ramp of 1 °C/min over a temperature range from 25 °C to 85 °C. Absorption was monitored at 260 nm. The melting temperatures (T_m) of squaraine-DNA constructs were determined from the first derivatives of sigmoidal melting curves. The visual inspection of the first derivative profile revealed the presence of a minor melting transition at a lower temperature (with the exception of **SQ-Sl$_3$** transverse dimer). As such, the main melting temperatures were determined by fitting two Gaussian curves to the first derivative in OriginPro 2019 (**Figs. S2** and **S3**).

The melting temperatures of squaraine-modified DNA HJs were compared with melting temperature of unlabeled HJ as a control.[1] The melting temperatures are summarized in **Table S1.**

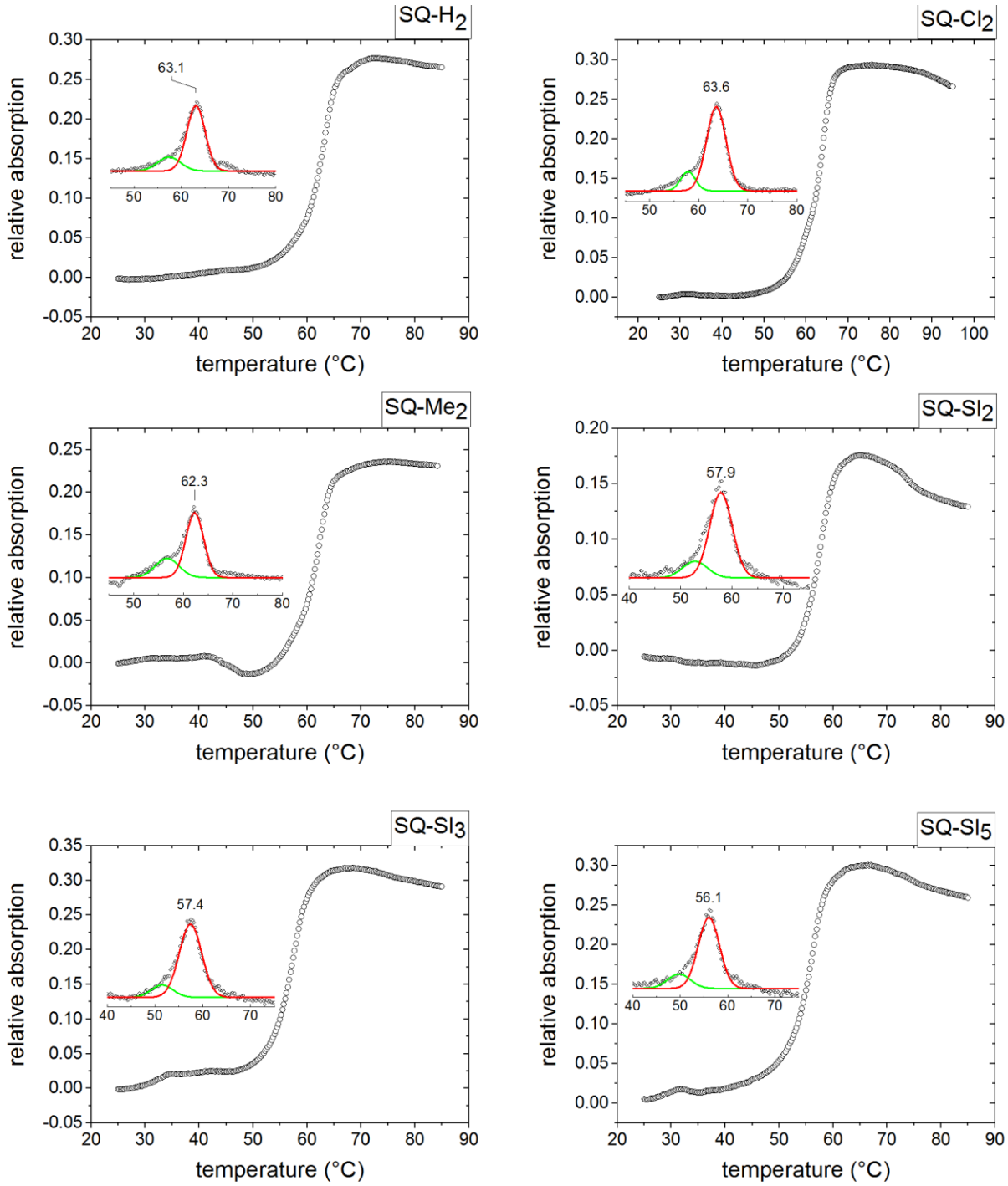

Figure S2. Melting profiles of squaraine adjacent dimers. The thermal denaturation was monitored in 1× TBE, 15 mM $MgCl_2$ containing 1.5 μM dye-DNA construct. The inserts show the first derivative as a function of temperature and fitted Gaussian curves.

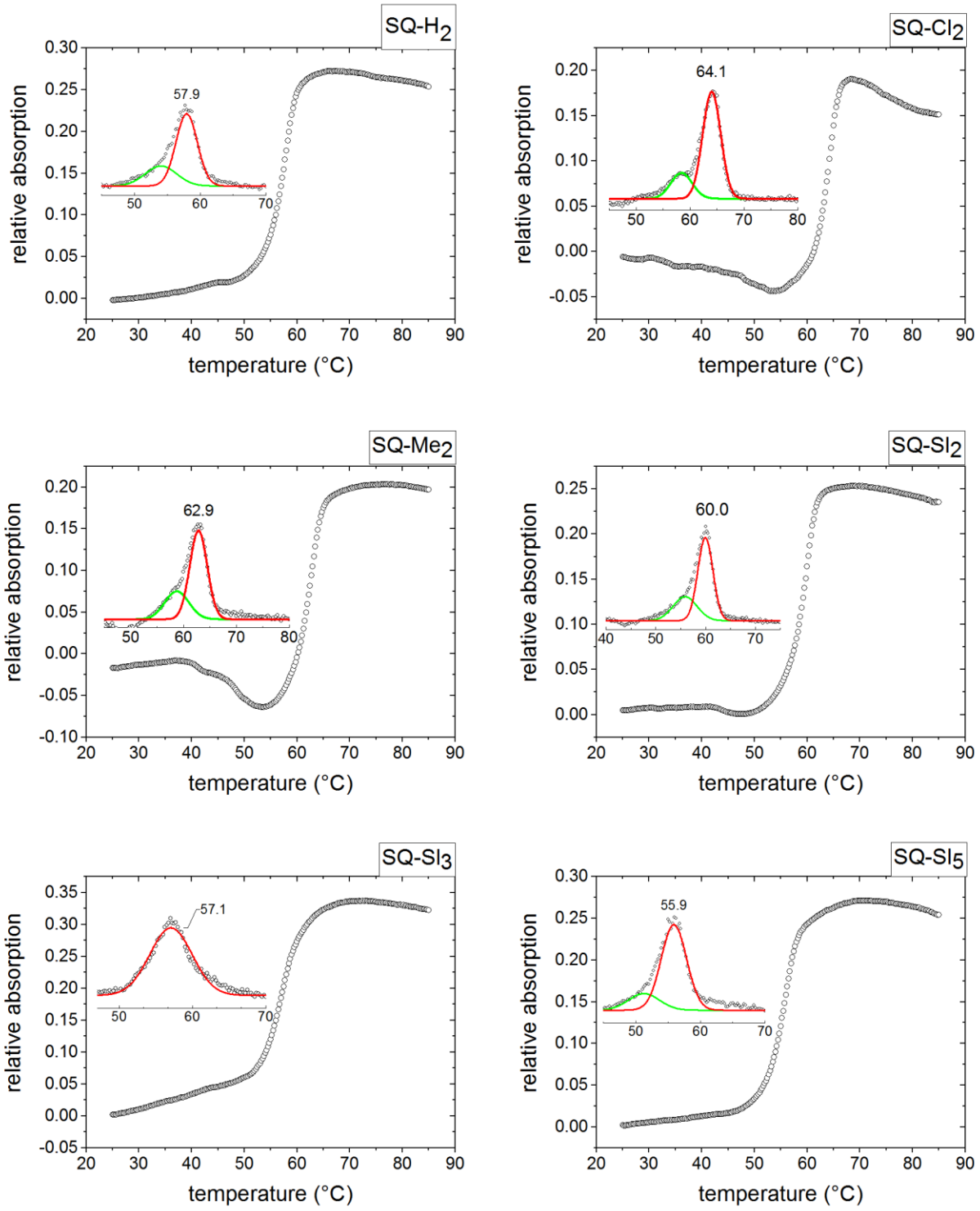

Figure S3. Melting profiles of squaraine transverse dimers. The thermal denaturation was monitored in 1× TBE, 15 mM $MgCl_2$ containing 1.5 μM dye-DNA construct. The inserts show the first derivative as a function of temperature and fitted Gaussian curves.

Table S1. Melting temperatures of Holliday Junctions with covalently attached squaraine dimers in 1× TBE, 15 mM $MgCl_2$.[a]

dye	$logP_{o/w}$	Adjacent Dimer		Transverse Dimer	
		$J_{1,2}$, meV	T_m, °C	$J_{1,2}$, meV	T_m, °C
SQ-Cl$_2$	5.31	132.2	63.6	79.6	64.0
SQ-Me$_2$	5.24	96.5	62.3	55.9	62.3
SQ-H$_2$	4.30	59.8	63.1	50.3	57.5
SQ-Sl$_2$	-3.66	64.3	57.9	71.3	59.5
SQ-Sl$_3$	-6.26	80.4	57.4	63.2	57.1
SQ-Sl$_5$	-11.82	97.9	56.1	77.5[b]	55.6

[a]The unlabeled DNA Holliday junction control had a T_m of 60.0 °C in 1× TBE, 15 mM $MgCl_2$.[1]
[b]modeling of experimental absorption and CD recorded at 5 °C.

Supporting Information 4: *Absorption of Squaraine Aggregates*

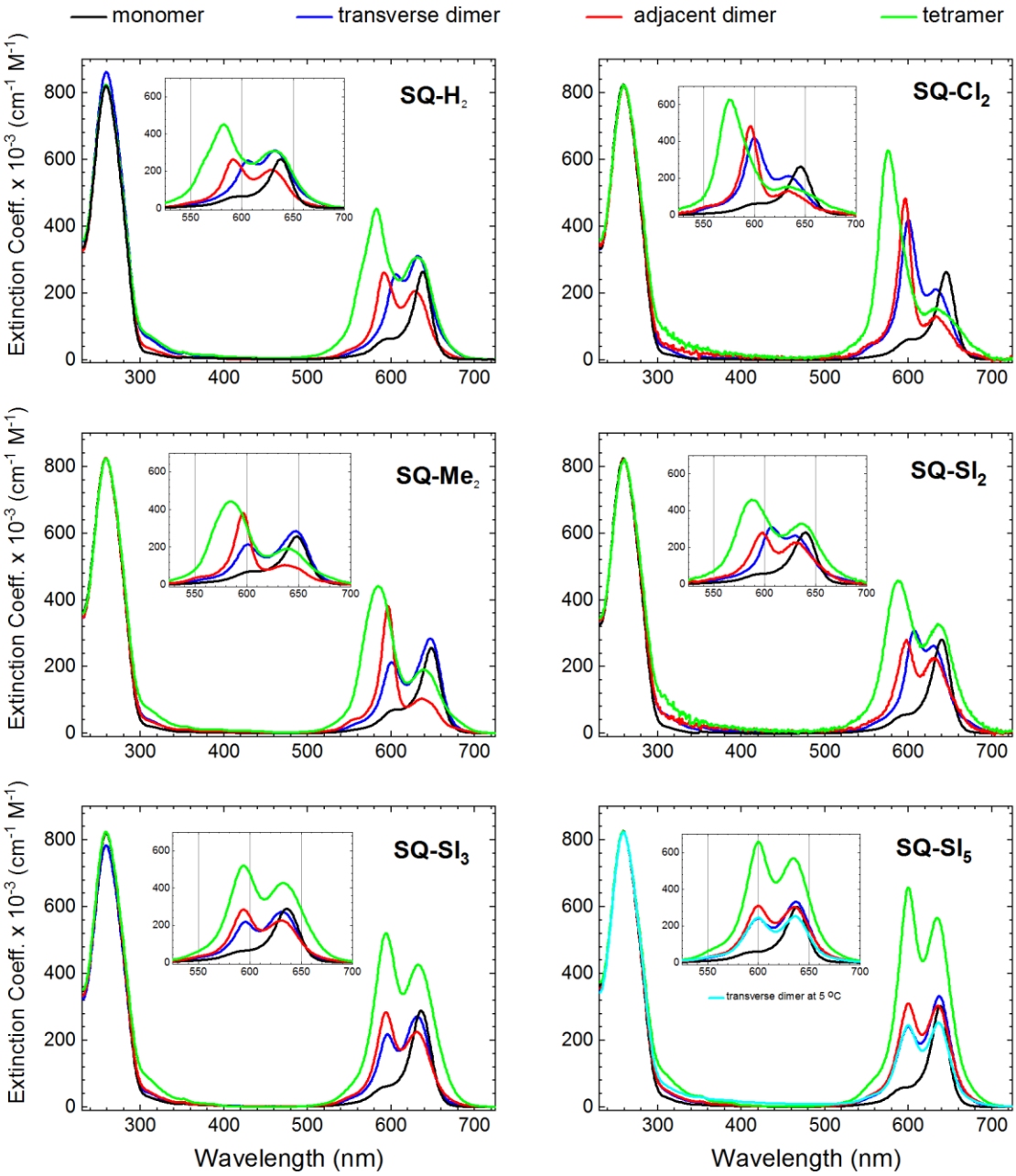

Figure S4. Acquired steady-state absorption spectra converted to extinction of squaraine-DNA constructs in 1× TBE, 15 mM $MgCl_2$ at room temperature. The squaraine-DNA construct concentration was 1.5 μM.

Supporting Information 5: *Monomer Fluorescence*

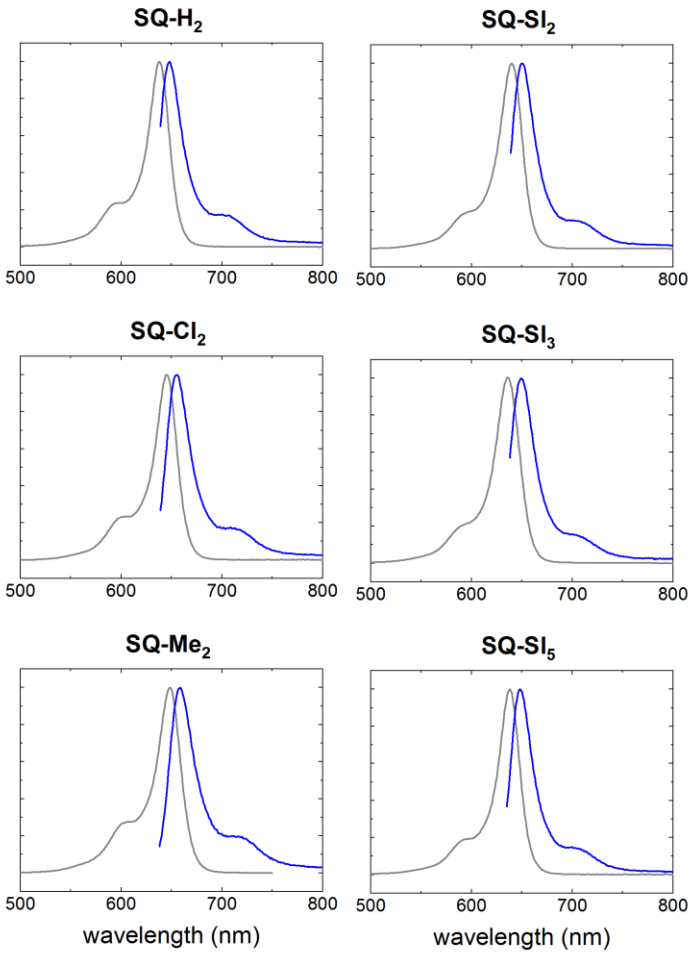

Figure S5. Squaraine monomer fluorescence normalized to dye peak maximum of squaraine-DNA constructs in 1× TBE, 15 mM $MgCl_2$ at room temperature. The squaraine-DNA construct concentration was 0.5 μM.

Table S2. Steady-State Absorption and Fluorescence Spectral Properties of Squaraine Monomers.

Monomer	$\lambda_{abs,max}$ (nm)	$FWHM_{abs,\ 0\text{-}0}$ (cm^{-1})	$\lambda_{em,max}$ (nm)	$FWHM_{em,\ 0\text{-}0}$ (cm^{-1})	λ_{Stokes} (cm^{-1})
SQ-H2	638	640	648	721	242
SQ-Cl2	645	664	656	686	260
SQ-Me2	648	685	659	781	258
SQ-Sl2	640	659	650	717	240
SQ-Sl3	636	719	649	773	315
SQ-Sl5	638	620	646	780	194

Supporting Information 6: *Fluorescence and Fluorescence Suppression in Squaraine Aggregates*

Fluorescence spectra were collected and scaled by the absorptance at the excitation maximum. The absorptance is defined as

$$A = 1 - T = 1 - 10^{-abs}$$

where A is absorptance at the excitation wavelength (λ_{exc}), T – transmitted light, and abs – absorption at λ_{exc}.
The area under emission curve of each aggregate was integrated in OriginPro2019. Obtained areas of integration were used to calculate fluorescence suppression according to the following formula:

$$\%FL\ Suppression = \frac{\int FL_{monomer} - \int FL_{aggregate}}{\int FL_{monomer}} \times 100\%$$

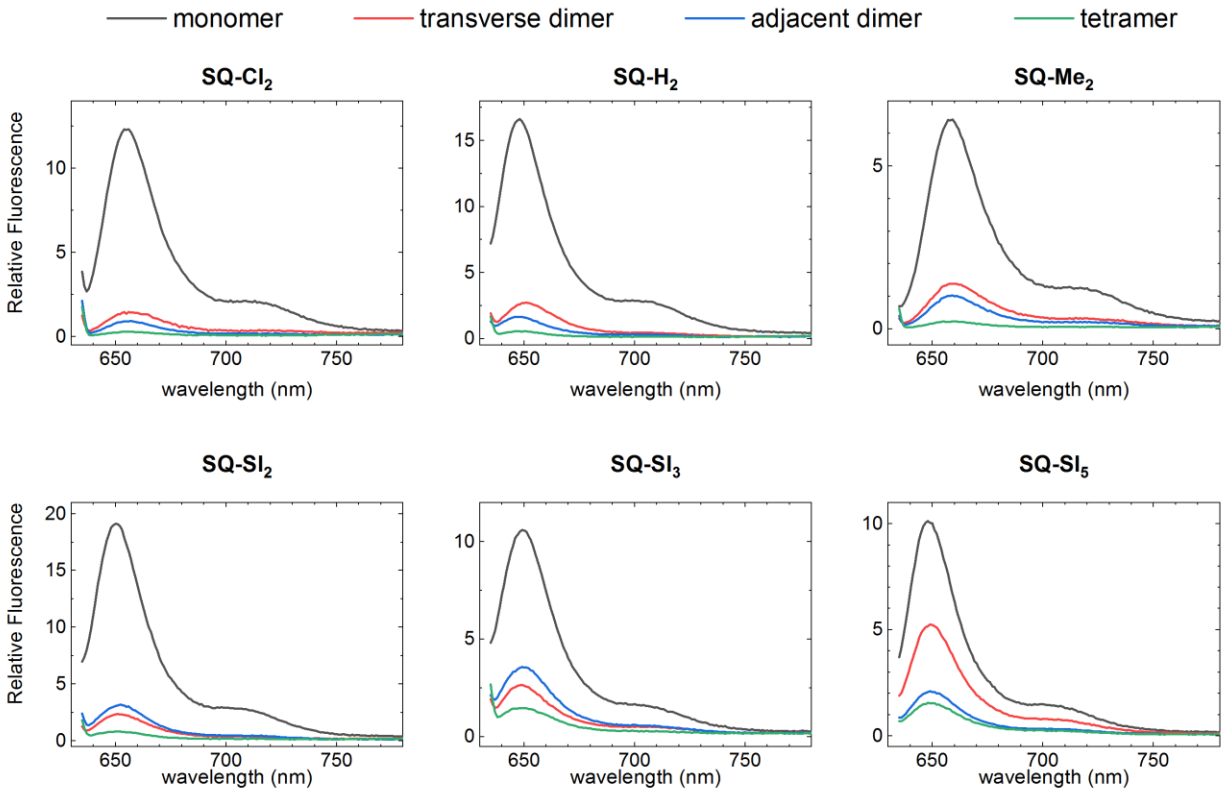

Figure S6. Scaled fluorescence emission of squaraine monomer, adjacent dimer, transverse dimer, and a tetramer recorded in 1× TBE, 15 mM $MgCl_2$ containing 0.5 µM HJ DNA construct at room temperature. The aggregates were excited at λ_{exc} = 630 nm. The fluorescence was normalized by the absorptance at the excitation wavelength.

Table S3. Fluorescence suppression of squaraine aggregates integrated in the range 639-800 nm.

Dye	Construct	Fluorescence peak maximum, nm	Area	FL Suppression %
SQ-Cl_2	monomer	656	1.92E+08	n/a
	trans. dimer	654	1.85E+07	90.36
	adj. dimer	657	1.42E+07	92.60
	tetramer	n/a	6.01E+06	96.86
SQ-Me_2	monomer	659	1.42E+08	n/a
	trans. dimer	659	3.55E+07	75.06
	adj. dimer	659	2.16E+07	84.81
	tetramer	659	6426648	95.48
SQ-H_2	monomer	648	2.38E+08	n/a
	trans. dimer	651	3.86E+07	83.75
	adj. dimer	646	2.26E+07	90.48
	tetramer	650	1.00E+07	95.77
SQ-Sl_3	monomer	649	1.49E+08	n/a
	trans. dimer	649	3.78E+07	74.66
	adj. dimer	649	4.55E+07	69.51
	tetramer	649	1.78E+07	88.05
SQ-Sl_2	monomer	650	2.28E+08	n/a
	trans. dimer	651	2.91E+07	87.28
	adj. dimer	652	3.57E+07	84.37
	tetramer	651	1.04E+07	95.44
SQ-Sl_5	monomer	648	1.56E+08	-
	trans. dimer	649	8.06E+07	48.44
	adj. dimer	649	3.33E+07	78.68
	tetramer	648	2.02E+07	87.08

Supporting Information 7: *Circular Dichroism Full Spectra*

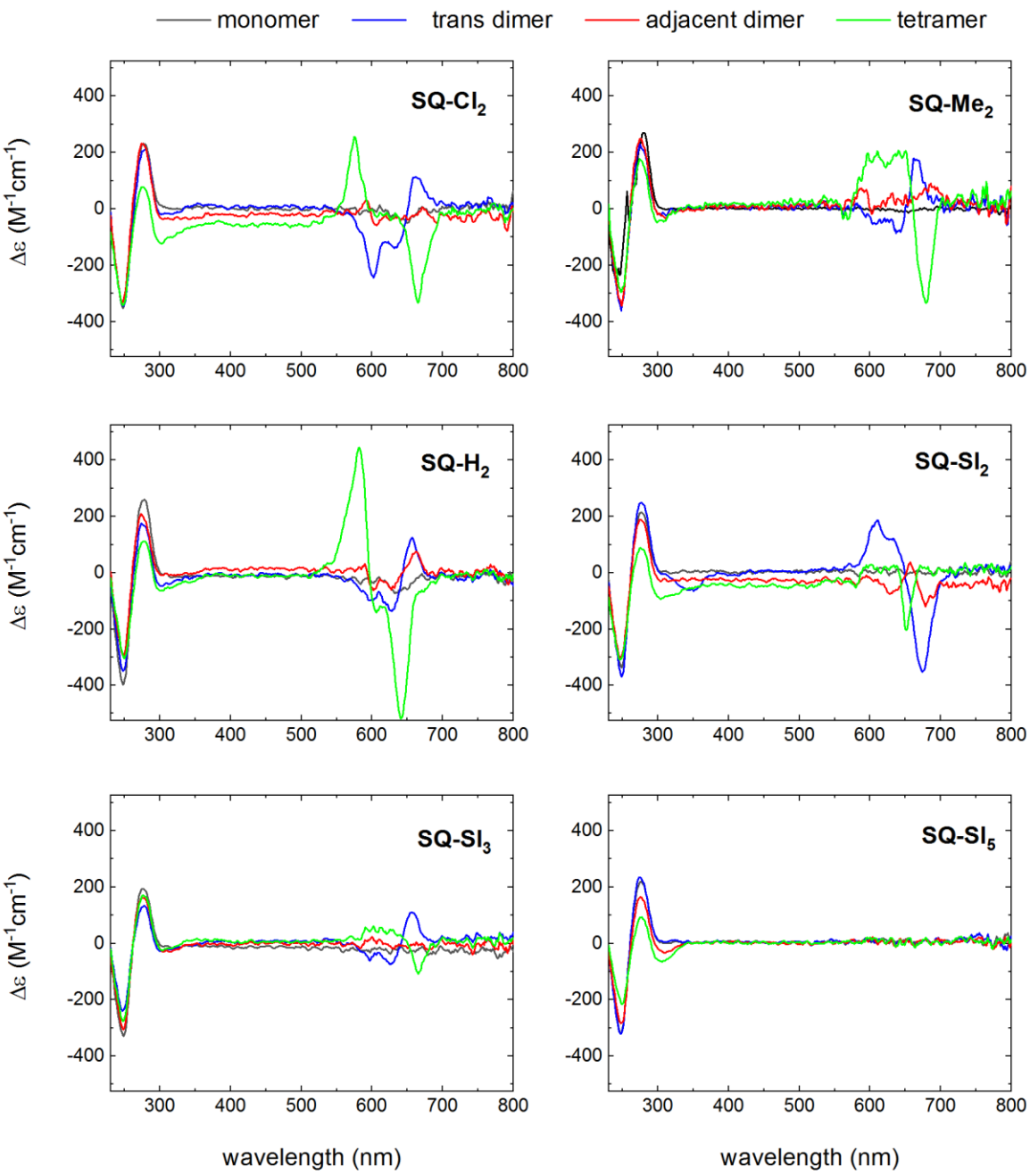

Figure S7. Acquired full CD spectra of the squaraine-DNA constructs recorded in 1× TBE, 15 mM $MgCl_2$ at room temperature. The squaraine-DNA construct concentration was 1.5 μM.

Supporting Information 8: *Fitting Absorption and CD using KRM Model*

When intermolecular distances are much greater than dye size, the excitonic hopping parameter $J_{m,n}$ can be expressed in a point dipole-dipole interaction form[2-4] representing the interaction between a pair of molecular transition dipoles μ_m and μ_n for the dyes at sites *m* and *n*:

$$J_{m,n} = \frac{1}{4\pi\varepsilon\varepsilon_0}\left(\frac{\boldsymbol{\mu_m}\cdot\boldsymbol{\mu_n}}{|\boldsymbol{R_{m,n}}|^3} - \frac{(\boldsymbol{\mu_m}\cdot\boldsymbol{R_{m,n}})(\boldsymbol{\mu_n}\cdot\boldsymbol{R_{m,n}})}{|\boldsymbol{R_{m,n}}|^5}\right) \quad \text{(eq S1)}$$

where $\boldsymbol{R_{m,n}}$ – the position vector between the dye centers dyes *m* and *n*. (further $\boldsymbol{R_{1,2}}$ between two dyes)

In the extended dipole approximation,[5] the Coulomb energy between a pair of dipoles is given in Standard International units by:

$$J_{m,n} = \frac{\delta^2}{4\pi\epsilon_0\epsilon_r}\left(\frac{1}{|\boldsymbol{r_1}-\boldsymbol{r_2}|} - \frac{1}{|\boldsymbol{r_1}-\boldsymbol{s_2}|} - \frac{1}{|\boldsymbol{s_1}-\boldsymbol{r_2}|} + \frac{1}{|\boldsymbol{s_1}-\boldsymbol{s_2}|}\right) \quad \text{(eq S2)}$$

where δ is the oscillating point charge in Coulombs, ϵ_0 is the permittivity of the vacuum (ϵ_0 = $8.85 \times 10^{-12}\text{m}^{-3}\text{kg}^{-1}\text{s}^4\text{A}^2$), ϵ_r is the relative dielectric constant of the medium, $\boldsymbol{r_1}$ and $\boldsymbol{s_1}$ are the location of the "+" and "- "charges on molecule *1* and similarly for molecule *2*. The distance units are meters and the exchange energy $J_{m,n}$ unit are Joules.

The transition dipole moment is given by $\mu = \delta l$ where l is the distance in meters between the two point charges on a given molecule, and ϵ_r is given by $\epsilon_r = n^2$ where *n* is the index of refraction of the medium.

Then the equation (S2) can be rewritten as:

$$J_{12} = \frac{J_0}{l^2}\left(\frac{1}{|\boldsymbol{r_1}-\boldsymbol{r_2}|} - \frac{1}{|\boldsymbol{r_1}-\boldsymbol{s_2}|} - \frac{1}{|\boldsymbol{s_1}-\boldsymbol{r_2}|} + \frac{1}{|\boldsymbol{s_1}-\boldsymbol{s_2}|}\right) \quad \text{(eq S3)}$$

where $J_0 = \frac{\mu^2}{4\pi\epsilon_0 n^2}$ (eq S4)

The quantity J_0 has units of $\text{J}\cdot\text{m}^3$.

When the position vectors $\boldsymbol{r}$ and $\boldsymbol{s}$ are rewritten as:

$$\boldsymbol{r_1} = \boldsymbol{R_1} + \frac{l}{2}\boldsymbol{n_1} \qquad \boldsymbol{s_1} = \boldsymbol{R_1} - \frac{l}{2}\boldsymbol{n_1} \qquad \boldsymbol{r_2} = \boldsymbol{R_2} + \frac{l}{2}\boldsymbol{n_2} \qquad \boldsymbol{s_2} = \boldsymbol{R_2} - \frac{l}{2}\boldsymbol{n_2}$$

And when $|\boldsymbol{R_1} - \boldsymbol{R_2}| \gg l$, equation (eq S3) reduces to:

$$J_{12} = \frac{J_0}{|\boldsymbol{R_1}-\boldsymbol{R_2}|^3}[\boldsymbol{n_1}\cdot\boldsymbol{n_2} - 3(\boldsymbol{n_{12}}\cdot\boldsymbol{n_1})(\boldsymbol{n_{12}}\cdot\boldsymbol{n_2})] \quad \text{(eq S5)}$$

where $\boldsymbol{n_{12}} = \frac{\boldsymbol{R_1}-\boldsymbol{R_2}}{|\boldsymbol{R_1}-\boldsymbol{R_2}|}$

Thus, J_0 is the same constant in both the point dipole-dipole approximation and in the extended dipole approximation.

The theoretical absorbance as a function of energy, for comparison with experimental data, was computed from the line spectra obtained by diagonalizing the system Holstein-like Hamiltonian[6] by convolution with a Gaussian as:

$$A(E) = \sum_i \frac{\gamma_i}{\sqrt{2\pi\Gamma^2}} exp\ \left(-\frac{(E-E_i)^2}{2\Gamma^2}\right) \quad \text{(eq S6)}$$

Where the γ_i is the transition rates between the ground state E and the state having the eigenenergy E_i, and Γ is a linewidth.

Similarly, the CD absorbance as a function of energy was computed as:

$$A_{CD}(E) = \sum_i \frac{\gamma_i^{CD}}{\sqrt{2\pi\Gamma^2}} exp\left(-\frac{(E-E_i)^2}{2\Gamma^2}\right) \quad \text{(eq S7)}$$

The phenomenological constants used in the theoretical model are shown in **Tbl. S4.** To fit the monomer and then dimers and a tetramer data, we considered the length of the squaraine transition dipole moment to be 1.3 nm (which is slightly shorter than the length of an indolenine squaraine dye), the linewidth Γ to be 0.028-0.034 eV, and number of vibronic states n_v to be 3.

The transition dipole moment was determined using the following expression:[7]

$$M_{01} = 9.58 \times 10^{-2} \left(\frac{\left(2n^2+1\right)^2}{9n^3} \int \frac{\epsilon(\nu)}{\nu} d\nu\right)^{\frac{1}{2}} \quad \text{(eq S8)}$$

M_{01} – transition dipole moment in Debye; n - refractive index of water (n_{water} = 1.3327).

Note that μ has units of Coulomb meters while M_{01} has units of Debye. The conversion relation between the two is 1 Debye = 3.33564 × 1030 C·m.

The values of characteristic exciton hopping parameter J_0 calculated from M_{01} according to the equation (S4) are reported in **Table S5**, and its values was used as a fitting parameter in the calculations of squaraine dimers and a tetramers.

As a measure the goodness of the fits, we evaluated the overlap integrals of the experimental spectra with the theoretical spectra (**Tbl. S6**). Letting $\int S_{ab,ex}(E), S_{ab,th}(E)$, $S_{cd,ex}(E), and\ S_{cd,th}(E)$ denote respectively the experimental absorbance spectrum, theoretical absorbance spectrum, experimental CD spectrum, and theoretical CD spectrum where $\boldsymbol{E}$ is energy, the normalized absorbance overlap integral OI_{AB} of the spectrum is defined by:

$$OI_{AB} = \frac{\int S_{ab,ex}(E) S_{ab,th}(E) dE}{\sqrt{\int S_{ab,ex}^2(E) dE}\sqrt{\int S_{ab,th}^2(E) dE}} \quad \text{(eq S9)}$$

and the normalized overlap integral for the CD spectrum OI_{CD} is defined by:

$$OI_{CD} = \frac{\int S_{cd,ex}(E) S_{cd,th}(E) dE}{\sqrt{\int S_{cd,ex}^2(E) dE}\sqrt{\int S_{cd,th}^2(E) dE}} \quad \text{(eq S10)}$$

As an overall goodness parameter, we introduce:

$$OI_{tot} = \frac{1}{2}(OI_{ab} + OI_{cd}) \quad \text{(eq S11)}$$

In addition, mean-square deviation of absorbance and CD were utilized:

$ms_{abs} = \sum_i [S_{ab,ex}(E) - S_{ab,th}(E)]^2$ (eq S12)

$ms_{cd} = \sum_i [S_{cd,ex}(E) - S_{cd,th}(E)]^2$ (eq S13)

$Fitness = w_1(1 - r)^2 + w_2(1 - OI_{AB})^2 + w_3(1 - OI_{CD})^2 + w_4 ms_{abs} + w_5 ms_{cd}$ (eq S14)

where w_1, w_2, w_3, and w_4 are user selected weights. For a typical run the weights were chosen as $w_1 = 1$, $w_2 = w_3 = 0$, and $w_4 = w_5 = 1$.

The resulting outputs of the fit provide information regarding the angles and position of the dyes relative to each other. Given in spherical coordinates, the zenith (θ_i) and azimuth (φ_i) angles are given in degrees. The Cartesian components of the orientation vector for a dye are given in terms of θ_i and φ_i by the following set of equations:

$$n_x = \sin(\theta_i)\cos(\varphi_i),$$
$$n_y = \sin(\theta_i)\sin(\varphi_i),$$
$$n_z = \cos(\theta_i).$$

The positions of the dyes are given in nm and listed in **Tbl. S7.**

A center-to-center distance R between two dyes was calculated as:

$$R = \sqrt{(x_2 - x_1)^2 + (y_2 - y_1)^2 + (z_2 - z_1)^2}.$$

A slip angle θ_s was calculated as:

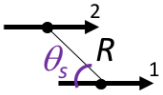

$$\theta_s = \cos^{-1}[\boldsymbol{n_1} \cdot \boldsymbol{n_{12}}]$$

Where $\boldsymbol{n_1}$ is a unit orientation vector given by:

$$\boldsymbol{n_1} = \sin(\theta_1)\cos(\varphi_1)\hat{x} + \sin(\theta_1)\sin(\varphi_1)\hat{y} + \cos(\theta_1)\hat{z}$$

And where $\boldsymbol{n_{12}}$ is a unit vector connecting dye centers is:

$$\boldsymbol{n_{12}} = \frac{1}{R_{1,2}}[(x_2 - x_1)\hat{x} + (y_2 - y_1)\hat{y} + (z_2 - z_1)\hat{z}]$$

The oblique angle between two vectors was calculated as:

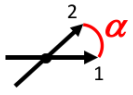

$$\alpha = \cos^{-1}[\sin(\theta_1)\sin(\theta_2)\cos(\varphi_1)\cos(\varphi_2) + \sin(\theta_1)\sin(\theta_2)\sin(\varphi_1)\sin(\varphi_2) + \cos(\theta_1)\cos(\theta_2)].$$

Extracted $J_{m,n}$ values and calculated geometric parameters for dye aggregates are summarized in the **Tbls. S8 – S13**.

Table S4. Input fitting parameters used in calculations of squaraine aggregates.

parameter	**Monomer A**					
	SQ-Cl$_2$	**SQ-Me$_2$**	**SQ-H$_2$**	**SQ-Sl$_3$**	**SQ-Sl$_2$**	**SQ-Sl$_5$**
The energy of vibron $E_{v,}$ *eV*	0.15	0.171	0.123	0.165	0.14	0.17
Displacement of excited state vibronic potential *d*, dimensionless units	0.66	0.66	0.69	0.61	0.62	0.58
The energy loss damping constant Γ, eV	0.030	0.031	0.030	0.034	0.030	0.028
parameter	**Adjacent Dimer BC**					
	SQ-Cl$_2$	**SQ-Me$_2$**	**SQ-H$_2$**	**SQ-Sl$_3$**	**SQ-Sl$_2$**	**SQ-Sl$_5$**
Vibrational state Hilbert space n_v	3	3	3	3	3	3
Characteristic exciton hopping parameter J_0^*, eV·nm^3	0.051	0.055	0.049	0.061	0.054	0.056
The energy offset from monomer E$_{of,}$ eV	0.0	0.005	0.0	0.0	0.005	-0.015
The energy of vibrone $E_{v,}$ eV	0.15	0.171	0.123	0.165	0.14	0.17
Displacement of excited state vibronic potential *d*, dimensionless units	0.66	0.66	0.69	0.61	0.62	0.58
The energy loss damping constant Γ, eV	0.03	0.031	0.03	0.034	0.03	0.028
Length of the transition dipole moment, nm	1.3	1.3	1.3	1.3	1.3	1.3
Closest distance between the long axes of any pair of dyes, nm	0.34	0.34	0.34	0.34	0.30	0.34
parameter	**Transverse Dimer AC**					
	SQ-Cl$_2$	**SQ-Me$_2$**	**SQ-H$_2$**	**SQ-Sl$_3$**	**SQ-Sl$_2$**	**SQ-Sl$_5$**
Vibrational state Hilbert space n_v	3	3	3	3	3	3
Characteristic exciton hopping parameter J_0^*, eV·nm^3	0.051	0.055	0.049	0.061	0.054	0.056
The energy offset from monomer E$_{of,}$ eV	0.00	-0.017	-0.005	-0.013	0.005	-0.015
The energy of vibron $E_{v,}$ eV	0.15	0.171	0.123	0.165	0.14	0.17
Displacement of excited state vibronic potential *d*, dimensionless units	0.66	0.66	0.69	0.61	0.62	0.58
The energy loss damping constant Γ, eV	0.03	0.031	0.03	0.034	0.03	0.028

Length of the transition dipole moment, nm	1.3	1.3	1.3	1.3	1.3	1.3
Closest distance between the long axes of any pair of dyes, nm	0.34	0.34	0.34	0.34	0.34	0.34

parameter	**Tetramer**			
	SQ-Cl_2	**SQ-Me_2**	**SQ-H_2**	**SQ-Sl_2**
Vibrational state Hilbert space n_v	4	4	4	4
Characteristic exciton hopping parameter, J_0^*, eV·nm^3	0.051	0.055	0.049	0.054
The energy offset from monomer, $E_{of,}$ eV	0.012	0.005	0.008	0.007
The energy of vibrone $E_{v,}$ eV	0.15	0.171	0.123	0.14
Displacement of excited state vibronic potential d, dimensionless units	0.66	0.66	0.69	0.62
The energy loss damping constant Γ, eV	0.03	0.031	0.03	0.03
Length of the transition dipole moment, nm	1.3	1.3	1.3	1.3
Closest distance between the long axes of any pair of dyes, nm	0.34	0.34	0.34	0.34

*J_0 was calculated from the fitting monomer absorption spectrum and used as an input parameter in theoretical fitting of dimers and a tetramer.

Table S5. Output parameters extracted from calculations of the monomer templated in DNA HJ.

	SQ-Cl_2	**SQ-Me_2**	**SQ-H_2**	**SQ-Sl_3**	**SQ-Sl_2**	**SQ-Sl_5**
Dipole moment M_{01} (Debye)	12.04	12.49	11.85	13.12	12.39	12.64
Characteristic exciton hopping parameter J_0 (eV · nm^3)	0.051	0.055	0.049	0.061	0.054	0.056

Table S6. Goodness of the fit parameters for absorbance and CD spectra of squaraine aggregates.

Construct	r	OI_{AB}	OI_{CD}	OI_{Tot}	MSD_{abs}	MSD_{cd}	$w_{abscd}rms$
SQ-Cl$_2$ Adjacent dimer BC	1.04	0.95	0.36	0.65	0.42	9.19	9.61
SQ-Cl$_2$ Transverse dimer AC	1.00	0.98	0.79	0.89	0.27	2.62	2.89
SQ-Cl$_2$Tetramer	0.98	0.94	0.95	0.94	0.89	0.66	1.56
SQ-Me$_2$ Adjacent dimer BC	0.99	0.96	0.00	0.48	0.48	68.23	68.71
SQ-Me$_2$ Transverse dimer AC	1.01	0.96	0.89	0.92	1.11	1.17	2.27
SQ-Me$_2$ Tetramer	1.05	0.92	0.89	0.91	1.96	1.61	3.57
SQ-H$_2$ Adjacent dimer BC	0.99	0.89	0.83	0.86	1.93	2.32	4.26
SQ-H$_2$Transverse dimer AC	0.99	0.99	0.85	0.92	0.18	2.85	3.03
SQ-H$_2$Tetramer	1.00	0.98	0.98	0.98	0.56	0.33	0.89
SQ-Sl$_3$ Adjacent dimer BC	0.98	0.96	0.24	0.59	0.79	7.89	8.68
SQ-Sl$_3$ Transverse dimer AC	1.02	0.98	0.94	0.96	0.66	0.81	1.47
SQ-Sl$_2$ Adjacent dimer BC	1.00	0.95	0.18	0.57	0.89	11.34	0.00
SQ-Sl$_2$ Transverse dimer AC	0.99	0.96	0.98	0.94	0.54	0.74	1.28
SQ-Sl$_2$ Tetramer	1.09	0.93	0.74	0.83	2.21	1.77	3.98
SQ-Sl$_5$Adjacent dimer BC	1.03	0.93	0.00	0.47	1.77	67.43	1.77
SQ-Sl$_5$ Transverse dimer AC	0.99	0.95	0.11	0.53	1.46	10.05	1.46

r - the ratio of theoretical to experimental values of the ratio of the max abs CD peak height to max absorbance peak height

OI_{AB} - normalized overlap integral for the experimental and theoretical absorbance curves

OI_{CD} - normalized overlap integral for the experimental and theoretical CD spectra

OI_{tot} - mean of OI_{AB} and OI_{CD}

MSD_{abs} - absorbance spectrum mean-square deviation

MSD_{cd} - CD spectrum mean-square deviation

$w_{abscd}rms$ - weighted mean-squared deviation between the experimental and theoretical ABS and CD spectra

Table S7. Kühn-Renger-May model fitting outputs describing each dye orientation and position in squaraine aggregates.

Construct/Parameter	θ_i (°)	φ_i (°)	x_i (nm)	y_i (nm)	z_i (nm)
SQ-Cl$_2$ Adjacent Dimer BC					
Dye 1	88.56	-1.57	1.82	0.31	1.63
Dye 2	89.88	-1.25	1.79	-0..02	1.56
SQ-Cl$_2$ Transverse Dimer AC					
Dye 1	7.15	1.00	0.88	-0.15	0.01
Dye 2	-8.58	1.02	0.35	-0.27	-0.01
SQ-Cl$_2$ Tetramer					
Dye 1	89.36	0.00	1.82	-1.44	0.15
Dye 2	86.99	-2.82	1.18	-1.36	1.88
Dye 3	87.60	5.44	0.92	-0.94	2.06
Dye 4	91.29	-6.44	1.07	-1.26	2.34

Construct/Parameter	θ_i (°)	φ_i (°)	x_i (nm)	y_i (nm)	z_i (nm)
SQ-Me$_2$ Adjacent Dimer BC					
Dye 1	89.49	1.54	1.65	-0.97	1.25
Dye 2	87.11	1.87	1.89	-1.02	0.87
SQ-Me$_2$ Transverse Dimer AC					
Dye 1	76.52	28.44	2.52	0.32	1.47
Dye 2	99.10	-17.08	2.78	-0.46	1.00
SQ-Me$_2$ Tetramer					
Dye 1	90.69	-2.76	1.16	0.55	-0.05
Dye 2	82.45	-12.31	1.02	0.42	0.43
Dye 3	84.07	0.98	0.89	1.12	0.72
Dye 4	91.99	-7.76	0.69	0.86	0.95

Construct/Parameter	θ_i (°)	φ_i (°)	x_i (nm)	y_i (nm)	z_i (nm)
SQ-H$_2$ Adjacent Dimer BC					
Dye 1	104.50	4.77	1.85	-0.23	1.22
Dye 2	77.66	-14.11	1.76	0.18	0.60
SQ-H$_2$ Transverse Dimer AC					
Dye 1	-22.36	0.06	1.16	-0.45	0.28
Dye 2	25.14	-1.09	2.08	-0.43	0.40
SQ-H$_2$ Tetramer					
Dye 1	85.92	-0.77	0.28	-1.09	-0.02
Dye 2	95.07	-5.98	0.39	-1.27	0.42
Dye 3	88.61	-2.72	0.59	-1.21	0.84
Dye 4	91.07	0.54	2.02	-1.07	1.14

Construct/Parameter	θ_i (°)	φ_i (°)	x_i (nm)	y_i (nm)	z_i (nm)
SQ-Sl$_3$ Adjacent Dimer BC					
Dye 1	98.15	-14.99	2.44	-0.21	1.68
Dye 2	91.98	10.16	2.47	-0.86	1.49
SQ-Sl$_3$ Transverse Dimer AC					
Dye 1	-8.82	-0.36	1.53	-1.23	0.73
Dye 2	10.97	0.47	2.11	-1.16	1.03

Construct/Parameter	θ_i (°)	φ_i (°)	x_i (nm)	y_i (nm)	z_i (nm)
SQ-Sl$_2$ Adjacent Dimer BC					
Dye 1	110.47	18.77	1.62	-0.01	1.06
Dye 2	69.89	-7.95	1.44	0.43	0.30
SQ-Sl$_2$ Transverse Dimer AC					
Dye 1	4.58	0.55	0.17	-0.31	-0.35
Dye 2	-4.20	-0.67	-0.09	0.06	-0.06
SQ-Sl$_2$ Tetramer					
Dye 1	105.46	-1.03	1.22	-0.55	0.91
Dye 2	92.59	-16.24	1.09	-0.23	1.25
Dye 3	77.63	3.79	1.03	-0.19	1.87
Dye 4	91.33	1.29	0.06	-1.66	3.40

Construct/Parameter	θ_i (°)	φ_i (°)	x_i (nm)	y_i (nm)	z_i (nm)
SQ-Sl$_5$ Adjacent Dimer BC					
Dye 1	87.43	-4.40	2.79	-0.15	1.28
Dye 2	88.95	-3.15	2.83	0.19	0.87
SQ-Sl$_5$ Transverse Dimer AC					
Dye 1	70.56	-12.69	2.4	-0.20	1.33
Dye 2	99.87	6.01	2.4	0.20	0.66

Table S8. Calculated $J_{1,2}$ and geometric parameters for SQ **adjacent dimers**.

Dimer Aggregate	$J_{1,2}$ meV	Center-to Center distance R, Å	d_{min}, nm	Slip angle θ_s, °	Oblique angle α °
SQ-Cl$_2$	132.20	3.40	0.34	86.8	1.35
SQ-Me$_2$	96.50	4.47	0.36	59.0	2.40
SQ-H$_2$	59.80	7.52	0.34	32.7	32.70
SQ-Sl$_3$	80.40	6.71	0.34	25.8	25.80
SQ-Sl$_2$	64.3	8.90	0.30	75.0	48.3
SQ-Sl$_5$	97.9	4.76	3.6	89.2	2.0

Table S9. Calculated $J_{1,2}$ and geometric parameters for SQ **transverse dimers**.

Dimer Aggregate	$J_{1,2}$ meV	Center-to Center distance R, Å	d_{min}, nm	Slip angle θ_s, °	Oblique angle α °
SQ-Cl$_2$	79.6	5.45	0.35	81.8	15.70
SQ-Me$_2$	55.9	9.50	0.34	74.9	50.50
SQ-H$_2$	50.3	9.33	0.35	74.8	47.50
SQ-Sl$_3$	63.2	6.62	0.38	71.3	19.80
SQ-Sl$_2$	71.3	5.37	0.35	60.0	8.8
SQ-Sl$_5$	72.1	5.39	0.43	69.3	34.6

Table S10. Calculated $J_{m,n}$ and geometric parameters for **SQ-Cl$_2$ tetramer.**

Excitonic Hopping Parameter $J_{m,n}$ (meV)					
$J_{1,2}$	$J_{1,3}$	$J_{1,4}$	$J_{2,3}$	$J_{2,4}$	$J_{3,4}$
4.977	2.844	2.575	70.962	82.718	87.496
Center-to-Center Distance R (Å)					
$R_{1,2}$	$R_{1,3}$	$R_{1,4}$	$R_{2,3}$	$R_{2,4}$	$R_{3,4}$
18.501	21.740	23.228	5.2272	4.881	4.487
Oblique angle α (°)					
$\alpha_{1,2}$	$\alpha_{1,3}$	$\alpha_{1,4}$	$\alpha_{2,3}$	$\alpha_{2,4}$	$\alpha_{3,4}$
3.675	5.719	6.717	8.274	5.612	12.436
Slip angle θ_s (°)					
$\theta_{1,2}$	$\theta_{1,3}$	$\theta_{1,4}$	$\theta_{2,3}$	$\theta_{2,4}$	$\theta_{3,4}$
70.463	66.235	71.919	59.211	74.529	72.796

Table S11. Calculated $J_{m,n}$ and geometric parameters for **SQ-Me$_2$ tetramer.**

Excitonic Hopping Parameter $J_{m,n}$ (meV)					
$J_{1,2}$	$J_{1,3}$	$J_{1,4}$	$J_{2,3}$	$J_{2,4}$	$J_{3,4}$
84.103	25.179	15.531	42.719	38.016	103.360
Center-to-Center Distance R (Å)					
$R_{1,2}$	$R_{1,3}$	$R_{1,4}$	$R_{2,3}$	$R_{2,4}$	$R_{3,4}$
5.165	9.948	11.549	7.653	7.619	4.046
Oblique angle α (°)					
$\alpha_{1,2}$	$\alpha_{1,3}$	$\alpha_{1,4}$	$\alpha_{2,3}$	$\alpha_{2,4}$	$\alpha_{3,4}$
12.600	7.606	5.168	13.297	10.574	11.794
Slip angle θ_s (°)					
$\theta_{1,2}$	$\theta_{1,3}$	$\theta_{1,4}$	$\theta_{2,3}$	$\theta_{2,4}$	$\theta_{3,4}$
74.168	72.349	64.390	72.709	58.059	62.797

Table S12. Calculated $J_{m,n}$ and geometric parameters for **SQ-H$_2$ tetramer.**

Excitonic Hopping Parameter $J_{m,n}$ (meV)					
$J_{1,2}$	$J_{1,3}$	$J_{1,4}$	$J_{2,3}$	$J_{2,4}$	$J_{3,4}$
77.769	24.765	5.138	85.103	9.799	50.909
Center-to-Center Distance R (Å)					
$R_{1,2}$	$R_{1,3}$	$R_{1,4}$	$R_{2,3}$	$R_{2,4}$	$R_{3,4}$
4.869	9.198	20.951	4.640	17.899	14.685
Oblique angle α (°)					
$\alpha_{1,2}$	$\alpha_{1,3}$	$\alpha_{1,4}$	$\alpha_{2,3}$	$\alpha_{2,4}$	$\alpha_{3,4}$
10.528	3.319	5.309	7.237	7.641	4.076
Slip angle θ_s (°)					
$\theta_{1,2}$	$\theta_{1,3}$	$\theta_{1,4}$	$\theta_{2,3}$	$\theta_{2,4}$	$\theta_{3,4}$
72.151	65.987	29.645	70.846	25.512	13.285

Table S13. Calculated $J_{m,n}$ and geometric parameters for **SQ-Sl$_2$ Tetramer.**

Excitonic Hopping Parameter $J_{m,n}$ (meV)					
$J_{1,2}$	$J_{1,3}$	$J_{1,4}$	$J_{2,3}$	$J_{2,4}$	$J_{3,4}$
72.618	27.639	0.001	57.425	1.576	2.415
Center-to-Center Distance R (Å)					
$R_{1,2}$	$R_{1,3}$	$R_{1,4}$	$R_{2,3}$	$R_{2,4}$	$R_{3,4}$
4.778	10.317	29.638	6.249	27.903	23.357
Oblique angle α (°)					
$\alpha_{1,2}$	$\alpha_{1,3}$	$\alpha_{1,4}$	$\alpha_{2,3}$	$\alpha_{2,4}$	$\alpha_{3,4}$
19.753	28.237	14.315	24.904	17.571	13.924
Slip angle θ_s (°)					
$\theta_{1,2}$	$\theta_{1,3}$	$\theta_{1,4}$	$\theta_{2,3}$	$\theta_{2,4}$	$\theta_{3,4}$
63.096	64.581	53.464	81.089	66.404	72.224

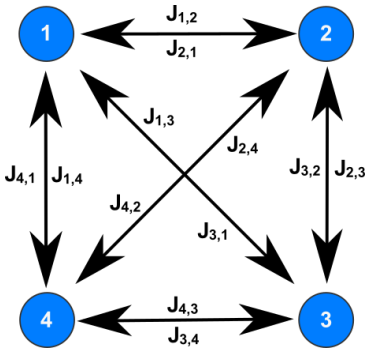

Figure S8. A matrix for excitonic hopping parameter $J_{m,n}$ in a tetramer.

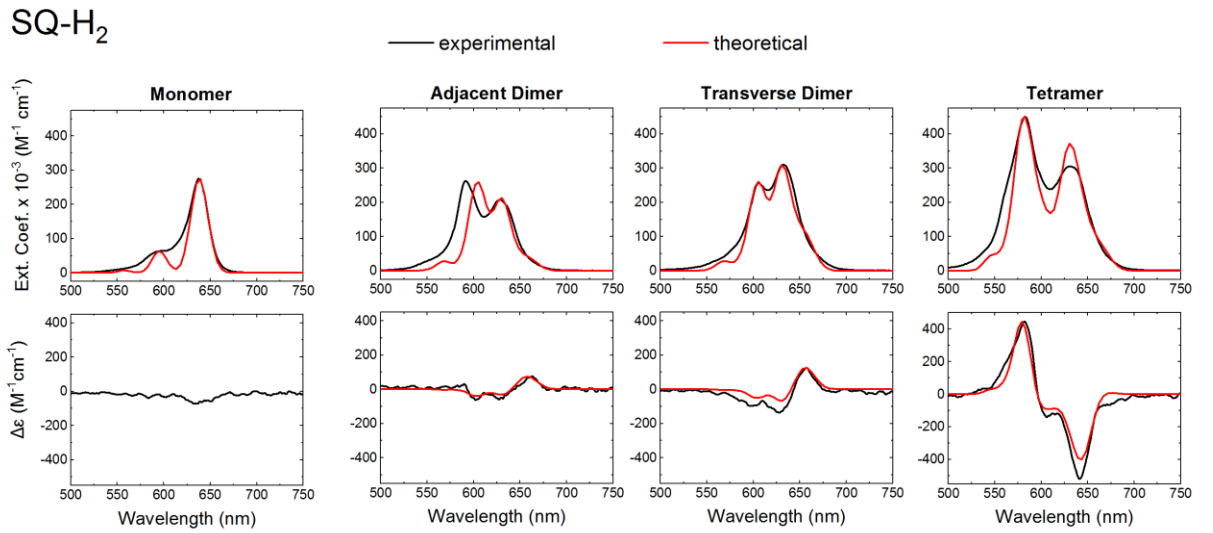

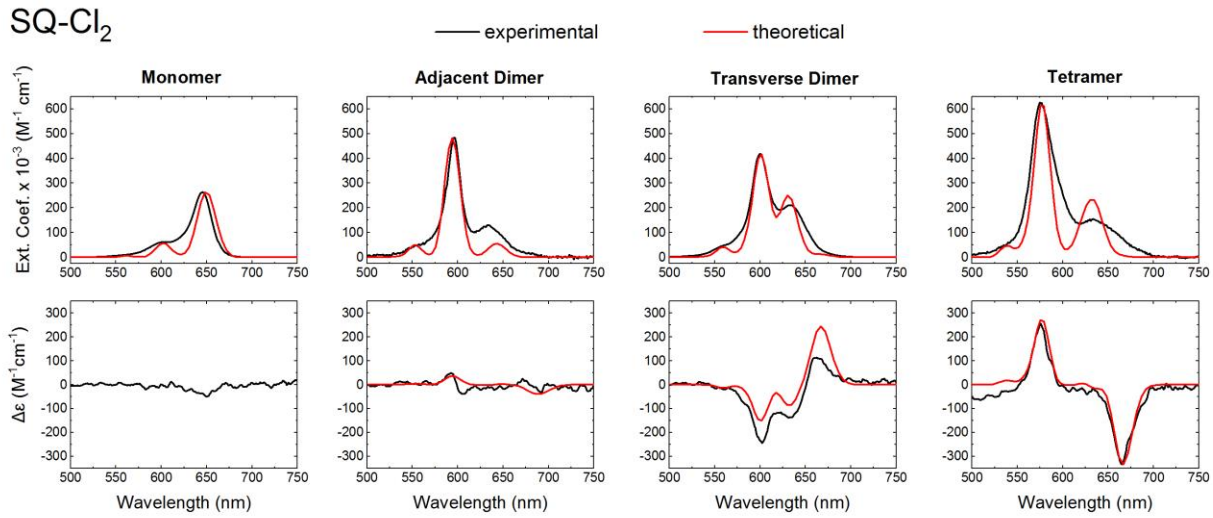

SQ-Me_2

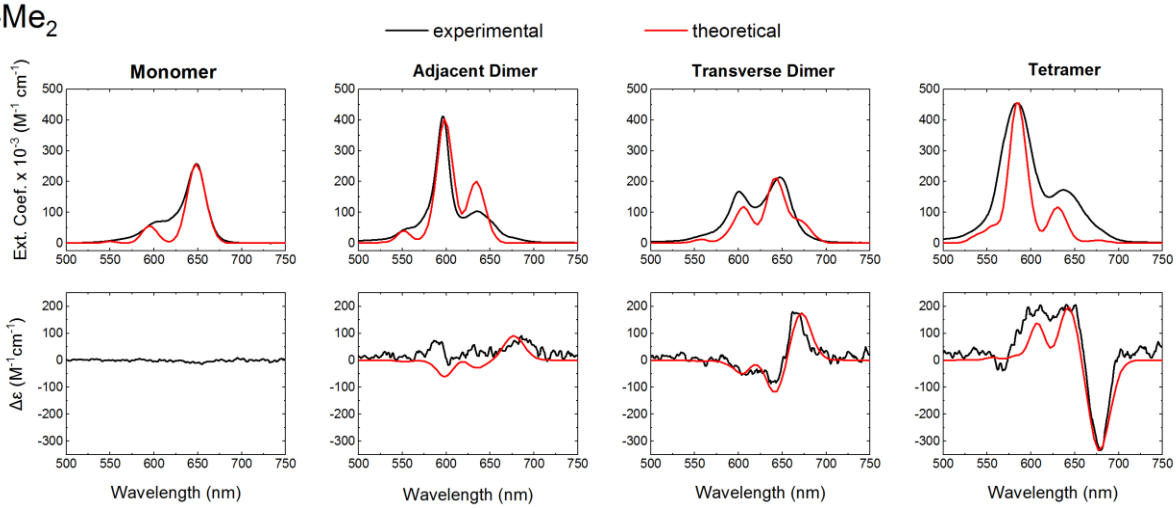

SQ-Sl_2

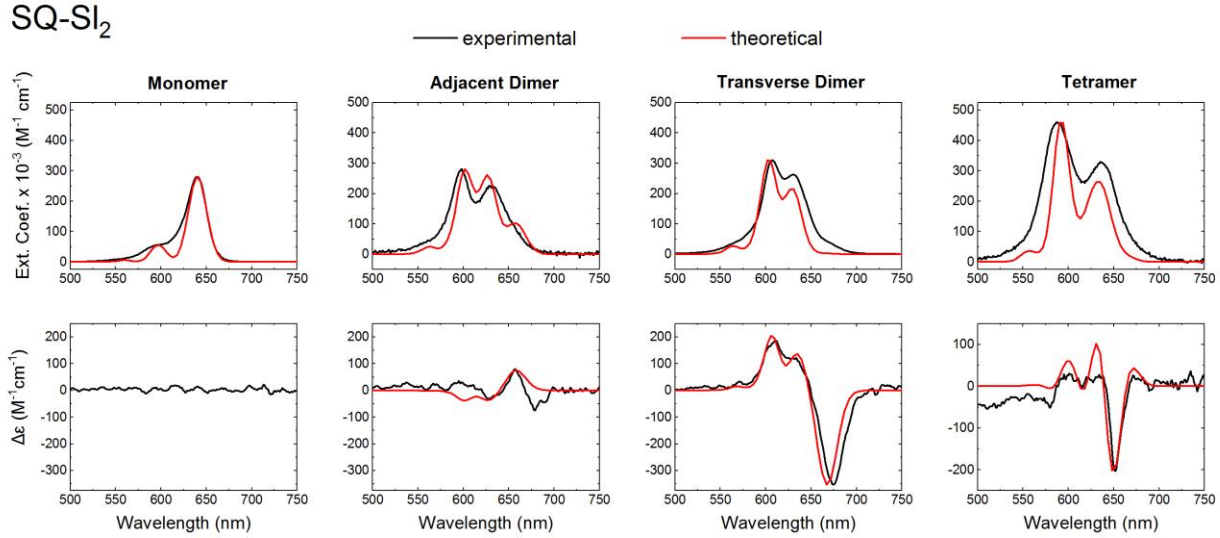

SQ-Sl_3

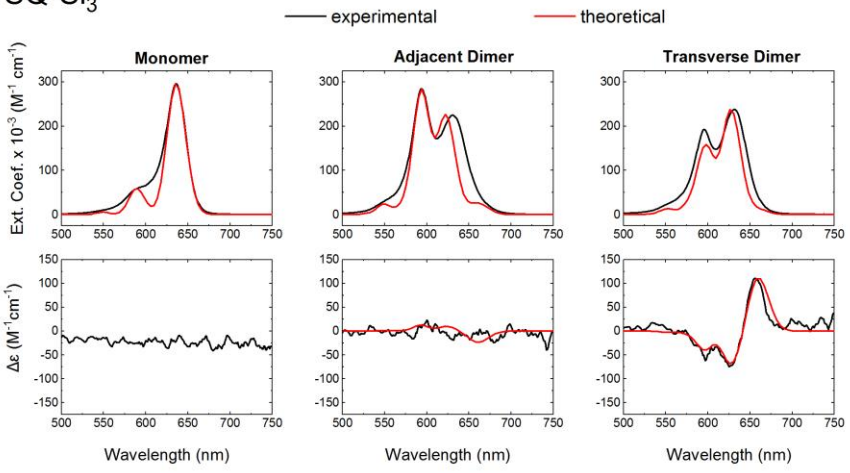

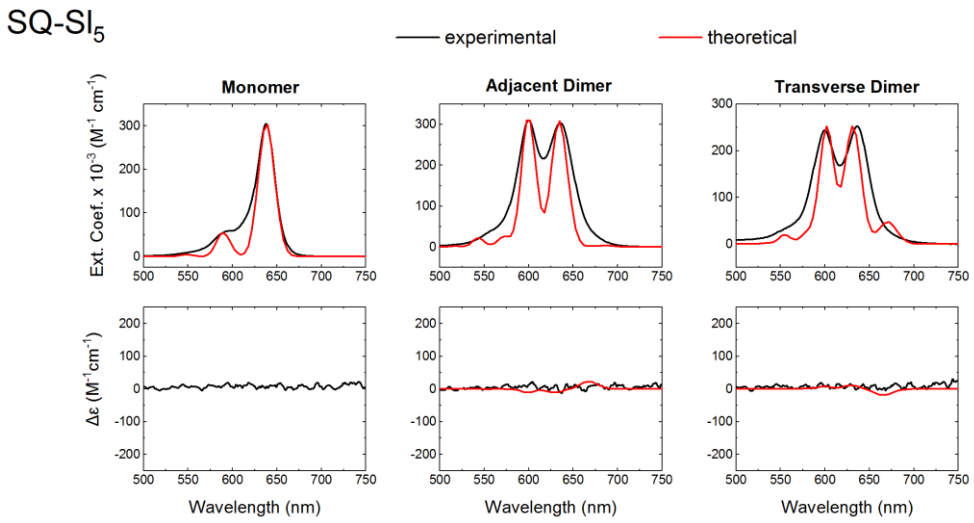

Figure S9. Acquired steady-state absorption and CD spectra of squaraine-DNA constructs in 1× TBE, 15 mM $MgCl_2$ at room temperature (black lines) and theoretical absorption spectra derived from KRM modeling (red lines). The squaraine-DNA construct concentration was 1.5 μM.

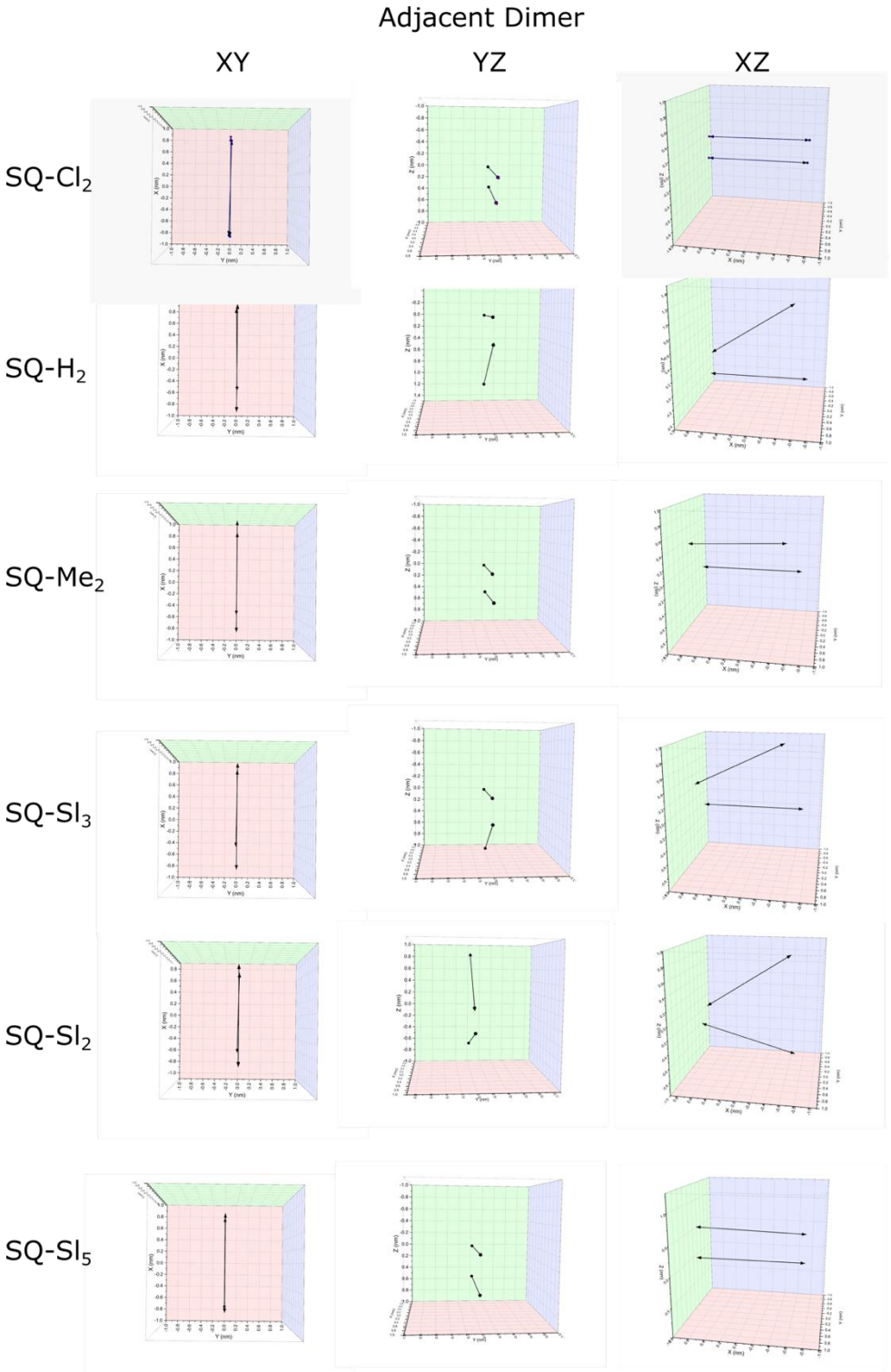

Figure S10. Transition dipole moments derived from the KRM modeling of the absorption and CD spectra of squaraines in the adjacent dimer configuration. The transition dipole moments corresponding to each dye in a dimer are shown as black double-headed arrows projected into the XY, YZ, and XZ planes.

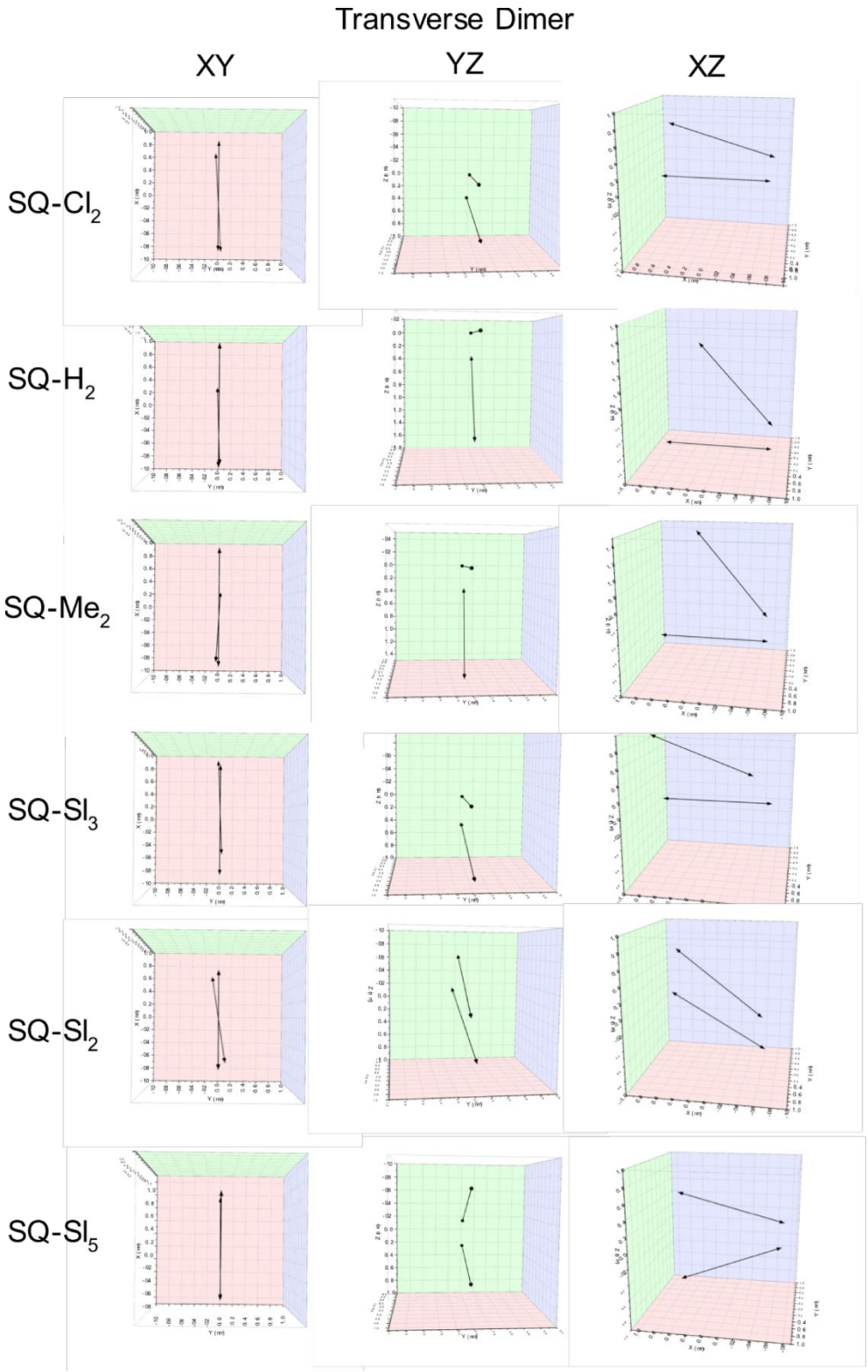

Figure S11. Transition dipole moments derived from the KRM modeling of the absorption and CD spectra of squaraines in the transverse dimer configuration. The transition dipole moments corresponding to each dye in a dimer are shown as black double-headed arrows projected into the XY, YZ, and XZ planes.

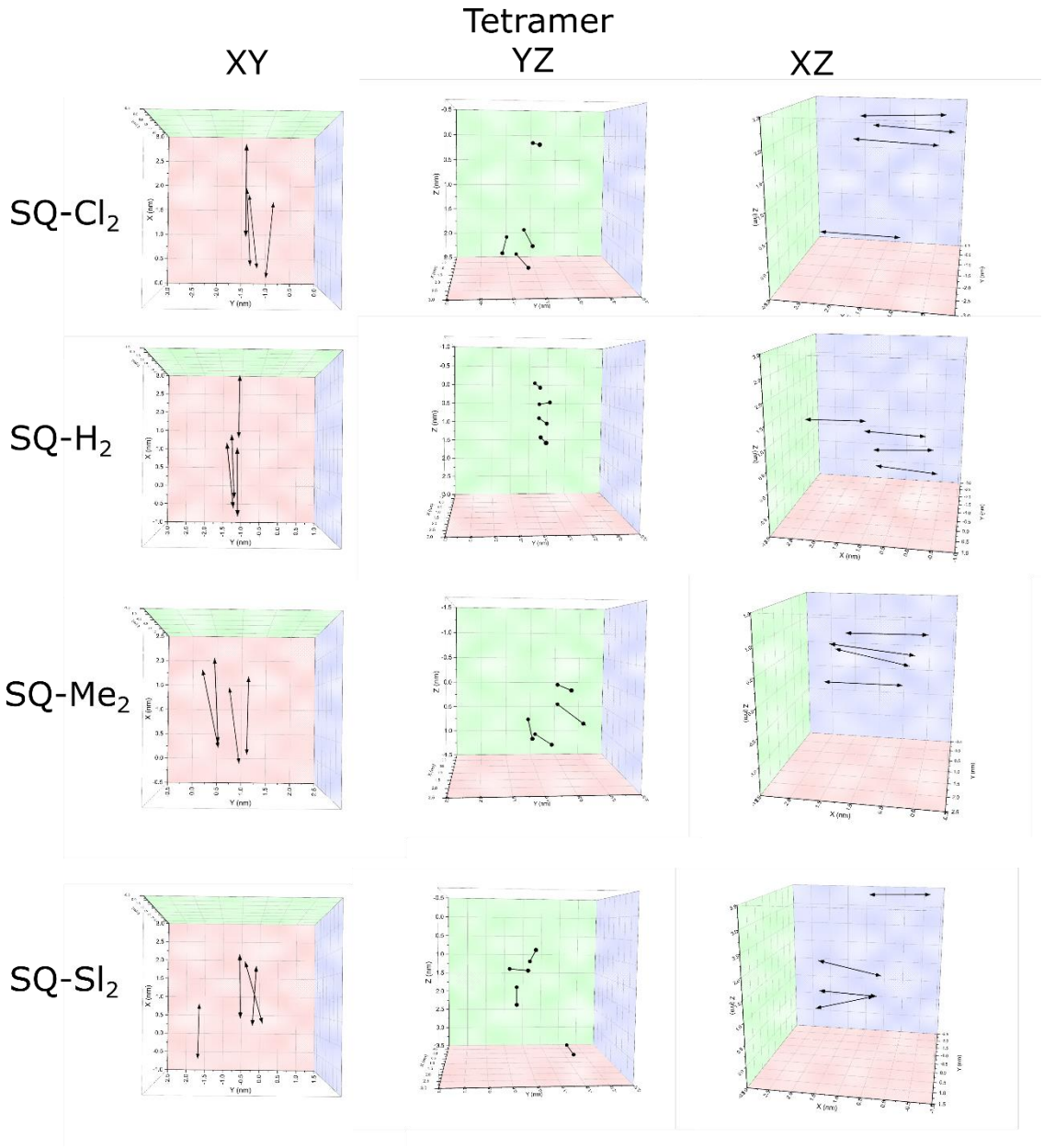

Figure S12. Transition dipole moments derived from the KRM modeling of the absorption and CD spectra of squaraines in the tetramer configuration. The transition dipole moments corresponding to each dye in a tetrame are shown as black double-headed arrows projected into the XY, YZ, and XZ planes.

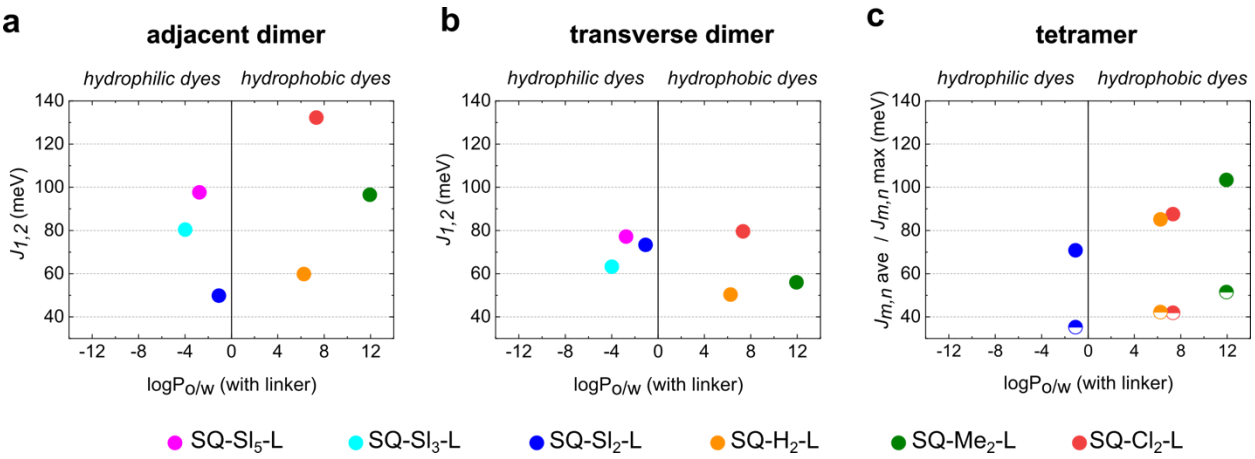

Figure S13. KRM values of $J_{1,2}$ in adjacent (**a**) and transverse (**b**) dimers. KRM values of $J_{m,n}$ maximum value (solid circles) and $J_{m,n}$ average (half solid circles) in squaraine tetramers plotted against partitioning of squaraine dyes (**c**). Linkers are included in the calculation of partitioning.

Supporting Information 9: *Influence of Electrostatic Interactions*

To evaluate contribution of electrostatic forces on excitonic coupling strength in the squaraine aggregates, we calculated a ground state static dipole moment (a property responsible for permanent dipole-dipole interactions), polarizability (a property responsible for interactions involving induced dipoles), and surface area (a property related to polarizability and hydrophobic effect) in squaraine dyes. These properties were plotted as a function of $J_{1,2}$ (**Fig. S14**, **Tbl. S14**). We did not observe strong relationships between these properties and $J_{1,2}$ indicating that permanent dipole-dipole and induced-dipole interactions not being the major factors in excitonic coupling. The role of permanent dipole-dipole interactions appeared to be the least pronounced especially for the adjacent dimers because the excitonic coupling strength, in general, decreased as the static dipole increased (**Fig. S14a**). However, the squaraine **SQ-Sl2** with the highest static dipole moment warrants attention. With the strongest static dipole moment among the examined squaraines, **SQ-Sl2** exhibits a strong coupling (71.3 meV) in the transverse dimer configuration, and weaker coupling in the adjacent dimer configuration (64.3 meV). This can be explained with a parallel or antiparallel alignment of dyes maintained in each dimer configuration. In the transverse dimer, dyes might be forced (by a steric factor and/or DNA conformation) to adopt an antiparallel alignment which is beneficial for the dyes with a large static dipole in order to avoid repulsion and form attractive Coulomb interactions. And in the adjacent dimer, dyes might be forced to adopt a parallel alignment destabilizing the dimer if dye's static dipole moment is large. On the other hand, dyes with small static dipole like **SQ-H2**, **SQ-Cl2** and **SQ-Sl5** do not form strong dipole-dipole interactions and so less sensitive to dimer (anti)parallel alignment.

Polarizability responsible for induced-dipole interactions including dispersion appears to play a more prominent role for hydrophobic squaraines (**Fig. S14cd**). Comparable polarizabilities of hydrophilic dyes **SQ-Sl2**, **SQ-Sl3** and **SQ-Sl5** do not correlate with the difference in the excitonic coupling strength in their dimers. However, higher polarizability of **SQ-Cl2** and **SQ-Me2** compared to that of **SQ-H2** might explain stronger excitonic coupling in the dimers of the former.

Finally, larger surface areas of **SQ-Sl3** and **SQ-Sl5** might explain stronger coupling between these dyes than expected from their hydrophobicity (**Fig. S14ef**). Hydrophobic effect may play a

strong role in minimizing a large surface area of **SQ-Sl$_3$** and especially **SQ-Sl$_5$** while polar sulfo groups maintain contact with water.

Table S14. Physical properties of squaraines.

Dye	Static dipole, D	Polarizability, Å^3	Surface Area, Å^2
SQ-Cl$_2$	0.06	197	740
SQ-Me$_2$	0.53	197	735
SQ-H$_2$	0.26	192	665
SQ-Sl$_2$	3.88	205	825
SQ-Sl$_3$	3.45	205	920
SQ-Sl$_5$	1.36	203	1232

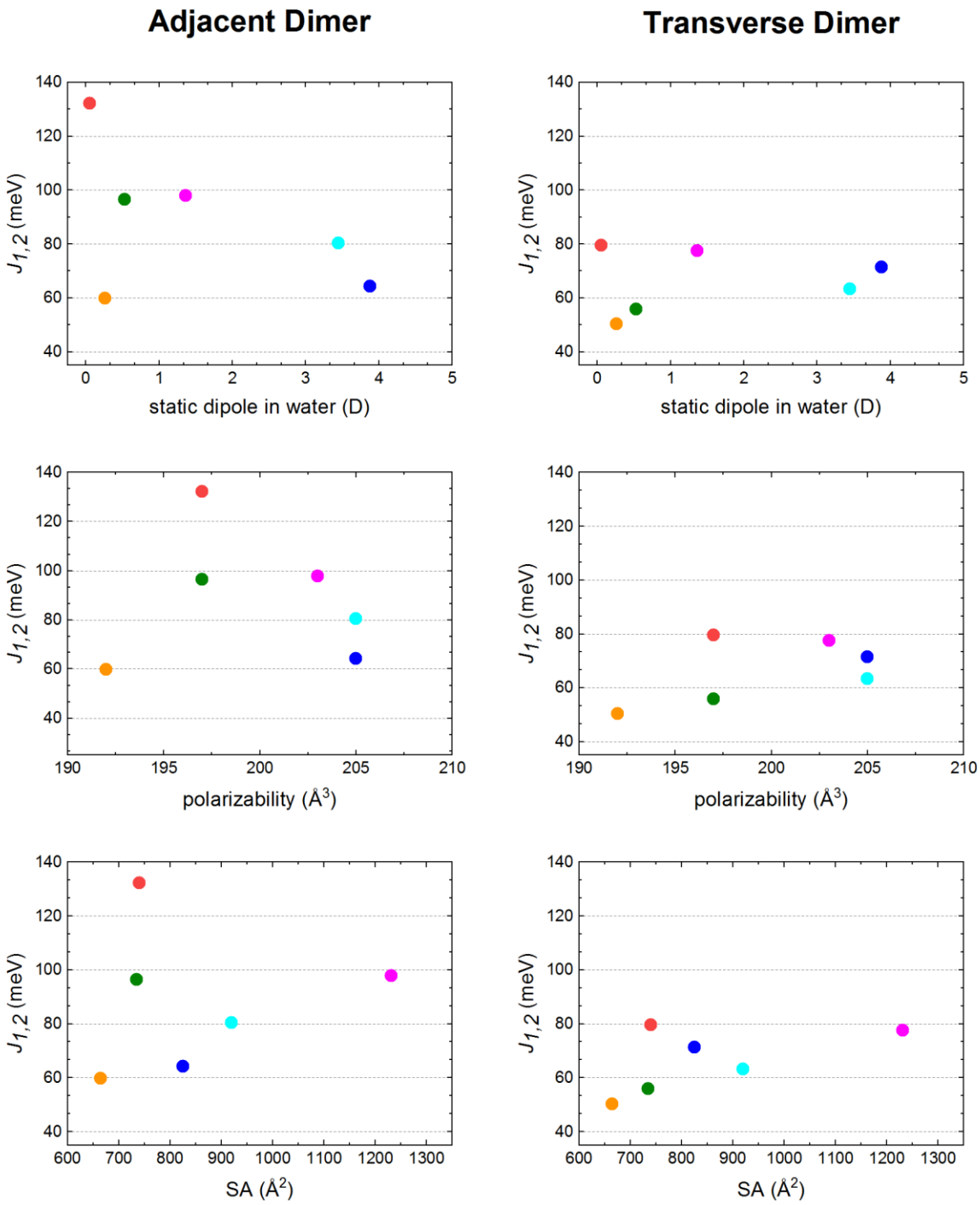

Figure S14. Relationships between squaraine physical properties and KRM-derived excitonic coupling strength $J_{1,2}$ in squaraine adjacent and transverse dimers. (**a, b**) Static dipole moment in water; (**c, d**) polarizability; and (**e, f**) surface area (SA).

In addition, we examined electron density distribution via electrostatic potential surfaces (**Fig. S15)**. The electrostatic potential is the energetic magnitude of interaction between a +1 positive charge and each point of molecular surface of constant electron density. In this regard, the

electrostatic potential surface serves as an equivalent to charge distribution. Electrostatic potentials revealed centrosymmetric electron density distribution in accordance with the D-A-D pattern characteristic for indolenine squaraines (where D is an electron-donor moiety and A is an electron-acceptor moiety). Squaraine **SQ-Cl$_2$** was characterized by the most neutral electrostatic potential surface and a lack of static dipole moment.

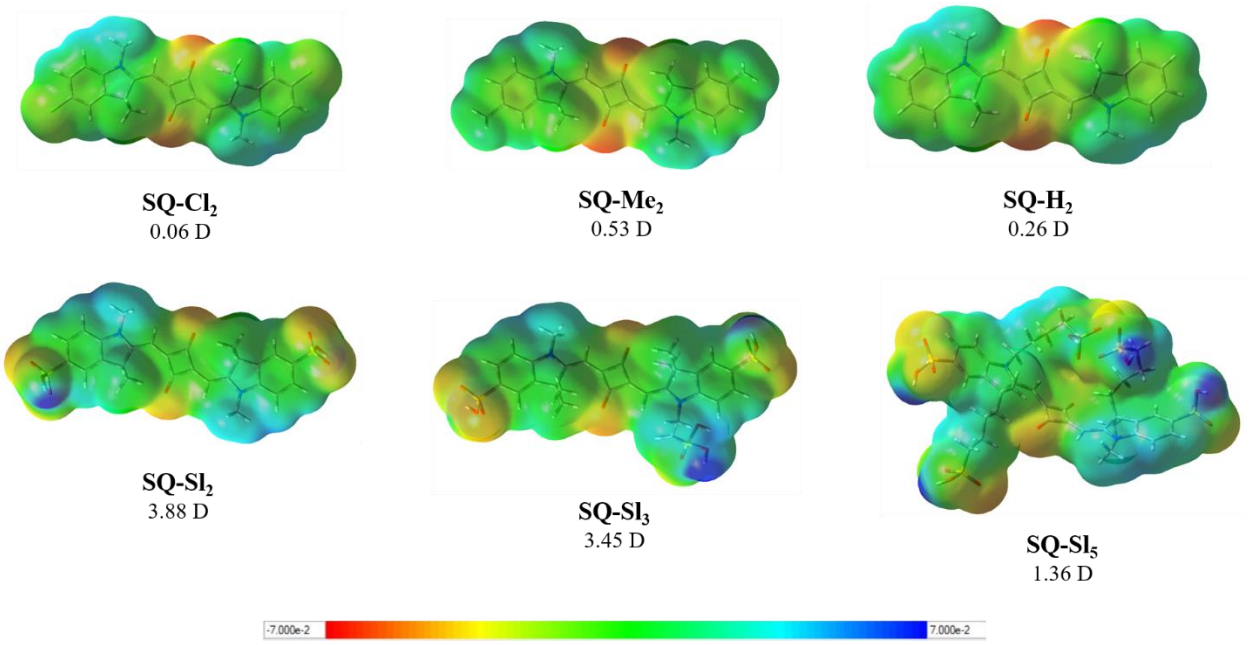

Figure S15. Electrostatic potential surfaces of custom squaraine dyes scaled to ±0.07 e/a.u.^{3}. Red is the most negative electrostatic potential, blue is the most positive electrostatic potential, and green is zero electrostatic potential. The values of ground state dipole moments in Debye calculated for dyes in water are provided.

All electrostatic potential surfaces and static polarizability data were generated via DFT using Gaussian16[8] and GaussView 5.0.9. Chemical structures of squaraine dyes were created in Avogadro software[9] where dye geometries were initially approximated using the universal force field (UFF).[10] Next, the molecular structures in gas state were optimized using M06-2X exchange correlation functional[11] and the 6-31+** basis set. To generate an electrostatic potential surface, a volume was generated using 80^3 points for the volume for both the electrostatic potential and electron density with a self-consistent field. The isosurface was generated using a molecular orbital isovalue of 0.02 e/a.u.^{3} with a density isovalue of 0.004 e/a.u.^{3} The color scale was fixed for all electrostatic potential surfaces with -7e-2 at the red value and 7e-2 at the blue value.

Supporting Information 10: *References*

1. Mass, O. A.; Wilson, C. K.; Roy, S. K.; Barclay, M. S.; Patten, L. K.; Terpetschnig, E. A.; Lee, J.; Pensack, R. D.; Yurke, B.; Knowlton, W. B. Exciton Delocalization in Indolenine Squaraine Aggregates Templated by DNA Holliday Junction Scaffolds. *J. Phys. Chem. B* **2020,** *124*, 9636-9647.
2. Abramavicius, D.; Palmieri, B.; Mukamel, S. Extracting Single and Two-Exciton Couplings in Photosynthetic Complexes by Coherent Two-Dimensional Electronic Spectra. *Chem. Phys.* **2008,** *357*, 79-84.
3. Abramavicius, D.; Mukamel, S. Exciton Dynamics in Chromophore Aggregates with Correlated Environment Fluctuations. *J. Chem. Phys.* **2011,** *134*, 174504.
4. Abramavicius, D.; Palmieri, B.; Voronine, D. V.; Šanda, F.; Mukamel, S. Coherent Multidimensional Optical Spectroscopy of Excitons in Molecular Aggregates; Quasiparticle Versus Supermolecule Perspectives. *Chem. Rev.* **2009,** *109*, 2350-2408.
5. Czikklely, V.; Forsterling, H. D.; Kuhn, H. Extended Dipole Model for Aggregates of Dye Molecules. *Chem. Phys. Lett.* **1970,** *6*, 207-210.
6. Holstein, T. Studies of Polaron Motion: Part I. The Molecular-Crystal Model. *Ann. Phys.* **1959,** *8*, 325-342.
7. Chung, P.-H.; Tregidgo, C.; Suhling, K. Determining a Fluorophore's Transition Dipole Moment from Fluorescence Lifetime Measurements in Solvents of Varying Refractive Index. *Methods and Applications in Fluorescence* **2016,** *4*, 045001.
8. Frisch, M. J.; Trucks, G. W.; Schlegel, H. B.; Scuseria, G. E.; Robb, M. A.; Cheeseman, J. R.; Scalmani, G.; Barone, V.; Petersson, G. A.; Nakatsuji, H., et al. *Gaussian 16 Rev. C.01*, Wallingford, CT, 2016.
9. Hanwell, M. D.; Curtis, D. E.; Lonie, D. C.; Vandermeersch, T.; Zurek, E.; Hutchison, G. R. Avogadro: An Advanced Semantic Chemical Editor, Visualization, and Analysis Platform. *J. Cheminf.* **2012,** *4*, 17.
10. Rappe, A. K.; Casewit, C. J.; Colwell, K. S.; Goddard, W. A.; Skiff, W. M. Uff, a Full Periodic Table Force Field for Molecular Mechanics and Molecular Dynamics Simulations. *J. Am. Chem. Soc.* **1992,** *114*, 10024-10035.
11. Zhao, Y.; Truhlar, D. G. The M06 Suite of Density Functionals for Main Group Thermochemistry, Thermochemical Kinetics, Noncovalent Interactions, Excited States, and Transition Elements: Two New Functionals and Systematic Testing of Four M06-Class Functionals and 12 Other Functionals. *Theor. Chem. Acc.* **2008,** *120*, 215-241.